Science
AAAS

Supplementary Materials for

In vivo multiplex imaging of dynamic neurochemical networks with designed far-red dopamine sensors

Yu Zheng *et al*.

Corresponding author: Yulong Li, yulongli@pku.edu.cn

Science **388**, eadt7705 (2025)
DOI: 10.1126/science.adt7705

The PDF file includes:

Other Supplementary Material for this manuscript includes the following:

Materials and Methods

Molecular biology

Plasmids were generated using the Gibson assembly method. Primers for PCR amplification of DNA fragments were synthesized (Ruibio Biotech) with 30-base pair overlap. The cDNA encoding D1R was cloned from the human GPCR cDNA library (hORFeome database 8.1), and the cDNA encoding cpHaloTag was synthesized (Shanghai Generay Biotech) based on the reported sequence(*23*). All constructs were verified using Sanger sequencing (Ruibio Biotech and Tsingke Biotech).

For screening and characterization in HEK293T cells, cDNAs encoding the candidate sensors were cloned into a modified pDisplay vector (Invitrogen) containing an upstream IgK leader sequence, followed by an IRES and membrane-anchored EGFP-CAAX for calibration. Site-directed mutagenesis was performed using primers with randomized NNS codons (32 codons in total, encoding all 20 possible amino acids). To measure the spectra, a stable cell line was generated by cloning the HaloDA1.0 gene into the pPacific vector, which contains a 3′ terminal repeat, IRES, the puromycin gene, and a 5' terminal repeat. For the luciferase complementation assay, the D1R/HaloDA1.0-SmBit construct was created by replacing the β2AR gene in β2AR-SmBit with D1R or HaloDA1.0, and miniGs-LgBit was generously provided by N. A. Lambert (Augusta University). For the Tango assay, D1R-Tango was cloned from the PRESTO-Tango GPCR Kit (Addgene kit no. 1000000068), and HaloDA1.0-Tango was generated by replacing D1R in D1R-Tango with HaloDA1.0. To compare brightness and labeling rates, cpHaloTag and HaloTag were fused to the C-terminus of D1R using a flexible GGTGGS linker. For characterization in cultured neurons, acute brain slices, and *in vivo* mouse experiments, the HaloDA1.0 and HaloDAmut sensors were cloned into the pAAV vector under the control of the human *Synapsin* promoter and used for AAV packaging. For zebrafish imaging, the HaloDA1.0 and HaloDAmut sensors were cloned into elavl3:Tet^{off} vectors, followed by P2A-EGFP or independent EGFP expression under the control of the zebrafish *myl7* promoter.

Preparation and fluorescence imaging of cultured cells

Cell culture and transfection

The HEK293T cell line was purchased from ATCC (CRL-3216) and cultured in high-glucose Dulbecco's Modified Eagle's Medium (Gibco) supplemented with 10% (v/v) fetal bovine serum (CellMax) and 1% penicillin-streptomycin (Gibco) at 37°C in humidified air containing 5% CO_2. For screening and characterizing the sensors, the cells were plated on 96-well plates and grown to 70% confluence before transfection with a mixture containing 0.3 μg DNA and 0.9 μg 40-kDa polyethylenimine (PEI) for 6-8 h. For kinetics measurements, cells were plated on 12-mm glass coverslips in 24-well plates and transfected with a mixture containing 1 μg DNA and 3 μg PEI for 6-8 h. Fluorescence imaging was conducted 24-36 h after transfection.

Rat primary cortical neurons were prepared from postnatal day 0 (P0) Sprague-Dawley rat pups (Beijing Vital River Laboratory) and dissociated using 0.25% trypsin-EDTA (Gibco). The neurons were plated on 12-mm glass coverslips coated with poly-D-lysine (Sigma-Aldrich) in 24-well plates and cultured with Neurobasal medium (Gibco) supplemented with 2% B-27 (Gibco), 1% GlutaMAX (Gibco), and 1% penicillin-streptomycin (Gibco) at 37 °C in humidified air containing 5% CO_2. Every 3 days, 50% of the media was replaced with fresh media. At 3 days in culture (DIV3), cytosine β-D-arabinofuranoside (Sigma) was added to the cortical cultures to a final

concentration of 1 μM. For characterization in cultured neurons, cortical cultures were transduced with adeno-associated virus (AAV) expressing HaloDA1.0 (full titer, 1 μl per well) at DIV6 and imaged at DIV15-20. For three-color neuron imaging, AAVs expressing HaloDA1.0, r5-HT1.0, and NE2m (full titer, 1 μl per well for each virus) were sequentially added to the cortical cultures at DIV6, DIV9, and DIV12, respectively, to minimize expression competition, and imaging was performed at DIV20-23.

Imaging of HEK293T cells

Before imaging, HEK293T cells expressing HaloDA1.0—or variants thereof—were pre-treated with 0.5-1 μM dye for 1 h, followed by washing with fresh culture medium for an additional 2 h. The culture medium was then replaced with Tyrode's solution consisting of (in mM): 150 NaCl, 4 KCl, 2 $MgCl_2$, 2 $CaCl_2$, 10 HEPES, and 10 glucose (pH adjusted to 7.35-7.45 with NaOH). HEK293T cells plated on 96-well CellCarrier Ultra plates (PerkinElmer) were imaged using the Operetta CLS high-content analysis system (PerkinElmer) equipped with a 20×, numerical aperture (NA 1.0) water-immersion objective and an sCMOS camera to record fluorescence. A 460-490-nm LED and 500-550-nm emission filter were used to image green fluorescence (e.g., EGFP); a 530-560-nm LED and 570-620-nm emission filter were used to image yellow fluorescence (e.g., JF525 and JF526); a 530-560-nm LED and 570-650 nm emission filter were used to image red fluorescence (e.g., JF585); a 615-645-nm LED and 655-760-nm emission filter were used to image far-red fluorescence (e.g., JF635, JF646, JFX650, and SiR650); and a 650-675-nm LED and 685-760-nm emission filter were used to image near-infrared fluorescence (e.g., SiR700).

For the measurement of labeling rate, HEK293T cells expressing HaloDA1.0, HaloDAmut, or other HaloTag variants were imaged for 3 frames with a 3-minute interval between frames prior to dye incubation. The medium was then replaced with fresh medium containing 1 μM of each dye. Twenty frames were acquired with a 3-minute interval, followed by another 20 frames with a 6-minute interval. Half of the HaloDA1.0-expressing cells were incubated with DA concurrently with the dye addition. D1R alone was used as a control to exclude background staining effects.

During imaging, the following compounds were applied via bath application at the indicated concentrations: DA (Sigma-Aldrich), SCH-23390 (MedChemExpress), eticlopride (Tocris), SKF-81297 (Tocris), quinpirole (Tocris), serotonin (Tocris), histamine (Tocris), octopamine (Tocris), tyramine (Sigma-Aldrich), ACh (Solarbio), γ-aminobutyric acid (Tocris), glutamate (Sigma-Aldrich), levodopa (Abcam), and NE (Tocris). The fluorescence signals produced by the HaloDA1.0 sensors were calibrated using EGFP, and the change was in fluorescence ($\Delta F/F_0$) was calculated using for formula $(F - F_0)/F_0$, where F_0 is the baseline fluorescence.

Imaging of cultured neurons

Before imaging, cultured neurons expressing HaloDA1.0 were pre-treated for 1 h with 1 μM JF635 or JF646, or with 200 nM SiR650 or JFX650 to minimize non-specific labeling. The dyes were then removed by washing the neurons with culture medium for an additional 2-3 h, and Tyrode's solution was used for imaging. The neurons, plated on 12-mm glass coverslips, were bathed in a custom-made chamber for imaging using an inverted A1R Si+ laser scanning confocal microscope (Nikon) equipped with a 20× (NA: 0.75) objective and a 40× (NA: 1.35) oil-immersion objective. A 488-nm laser and 525/50-nm emission filter were used to image green fluorescence (e.g., NE2m);

a 561-nm laser and 595/50-nm emission filter were used to image red fluorescence (e.g., r5-HT1.0); and a 640-nm laser and 700/75-nm emission filter were used to image far-red fluorescence (e.g., HaloDA1.0 labeled with JF635, JF646, SiR650, or JFX650). For single-color imaging, images were acquired with a frame interval of 5 s. For three-color imaging, the fluorescence signals from the green, red and far-red sensors were acquired sequentially, with a period interval of 5 s. The change in fluorescence ($\Delta F/F_0$) was calculated using the formula $(F - F_0)/F_0$.

Kinetics measurements

HEK293T cells expressing HaloDA1.0 were plated on 12-mm glass coverslips, labeled with JF646 or SiR650, and imaged using an A1R confocal microscope (Nikon) equipped with a 40× (NA: 1.35) oil-immersion objective. A glass pipette was positioned approximately 10-20 μm from the sensor-expressing cells, and fluorescence signals were recorded using the confocal high-speed line scanning mode at a scanning frequency of 1,024 Hz. To measure τ_{on}, 100 μM DA was puffed onto the cells from the pipette, and the resulting increase in fluorescence was fitted with a single-exponential function. To measure τ_{off}, 100 μM SCH-23390 was puffed onto cells bathed in 1 μM DA, and the resulting decrease in fluorescence was fitted with a single-exponential function.

Tango assay

HTLA cells stably expressing a tTA-dependent luciferase reporter and a β-arrestin2-TEV gene were a gift from B.L. Roth (University of North Carolina Medical School). The cells were initially plated in 6-well plates and transfected with either HaloDA1.0-Tango or D1R-Tango; 24 h after transfection, the cells were transferred to 96-well plates and incubated with varying concentrations of DA (ranging from 0.01 nM to 100 μM). In addition, 1 μM JF646 was applied to half of the wells transfected with HaloDA1.0-Tango. The cells were then cultured for 12 h to allow expression of tTA-dependent luciferase. Bright-Glo reagent (Fluc Luciferase Assay System, Promega) was added to a final concentration of 5 μM, and luminescence was measured 10 min later using a VICTOR X5 multi-label plate reader (PerkinElmer).

Mini G protein luciferase complementation assay

HEK293T cells were first plated in 6-well plates and co-transfected with a pcDNA3.1 vector expressing either HaloDA1.0-SmBit or D1R-SmBit (or empty vector) together with miniGs-LgBit; 24 h after transfection, the cells were dissociated and mixed with Nano-Glo Luciferase Assay Reagent (Promega) diluted 1,000-fold to a final concentration of 5 μM. The cell suspension was then distributed into 96-well plates and treated with various concentrations of DA. Following a 10-min incubation in the dark, luminescence was measured using a VICTOR X5 multi-label plate reader (PerkinElmer).

Spectra measurements

One-photon spectral characterization

The one-photon spectra were measured using a Safire 2 microplate reader (Tecan). HEK293T cells stably expressing HaloDA1.0 were plated in 6-well plates and labeled with dye after 24 h. The cells were then harvested and transferred to black 384-well plates. The fluorescence values measured in unlabeled cells were subtracted as background. Both the excitation and emission spectra were measured in the presence of saline or 100 μM DA at 5-nm increments. Below are the wavelength settings for each dye-labeled sample:

Dye labeling	Excitation spectra	Emission spectra
JF526	Ex: 300-570 nm; Em: 610 nm	Ex: 490 nm; Em: 520-700 nm
JF585	Ex: 450-640 nm; Em: 675 nm	Ex: 525 nm; Em: 570-800 nm
JF635, JF646, SiR650 and JFX650	Ex: 450-680 nm; Em: 720 nm	Ex: 580 nm; Em: 620-800 nm
SiR700	Ex: 500-760 nm; Em: 800 nm	Ex: 640 nm; Em: 680-800 nm

Two-photon spectral characterization

HEK293T cells expressing HaloDA1.0 were plated on 12-mm glass coverslips and labeled with JF646 or SiR650. Two-photon excitation spectra were measured at 10-nm increments ranging from 870 nm to 1300 nm using an Olympus FVMPE-RS microscope equipped with a tunable Spectra-Physics InSight X3 laser. The far-red signals were collected with a 660-750-nm emission filter and a 760-nm dichroic mirror positioned between the lasers and photomultiplier tubes (PMTs). The recorded signals were calibrated according to the output power of the tunable two-photon laser at each wavelength.

Synthesis of chemical dyes

Synthesis of SiR650-HTL

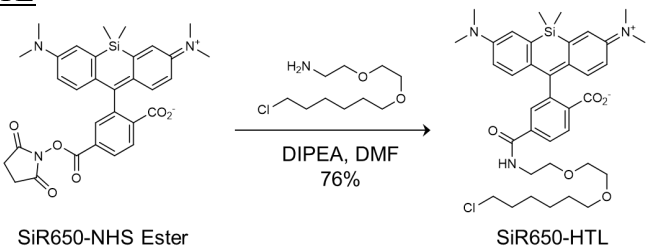

SiR650-NHS Ester SiR650-HTL

SiR-NHS Ester (23 mg, 40 μmol, 1.0 eq., obtained from CONFLUORE) and HaloTag(O2)amine (13 mg, 60 μmol, 1.5 eq.) were dissolved in 2 ml anhydrous DMF. DIPEA (13 μl, 80 μmol, 2.0 eq.) was then added, and the mixture was stirred at room temperature overnight. Purification of the mixture by reverse phase-HPLC (eluent, a 30-min linear gradient, from 20% to 95% solvent B; flow rate, 5.0 mL/min; detection wavelength, 650 nm; eluent A (ddH_2O containing 0.1% TFA (v/v)) and eluent B (CH_3CN)) provided SiR650-HTL (21 mg, 76% yield) as a blue solid.

^{1}H NMR (DMSO-d_6, 400 MHz) δ 8.78 (t, J = 5.5 Hz, 1H), 8.08 (dd, J = 8.0, 1.3 Hz, 1H), 8.02 (dd, J = 8.0, 0.4 Hz, 1H), 7.69 – 7.65 (m, 1H), 7.03 (d, J = 2.4 Hz, 2H), 6.65 (dd, J = 9.0, 2.6 Hz, 2H), 6.61 (d, J = 8.9 Hz, 2H), 3.57 (t, J = 6.7 Hz, 2H), 3.53 – 3.46 (m, 4H), 3.46 – 3.40 (m, 2H), 3.40 – 3.34 (m, 2H), 3.30 (t, J = 6.5 Hz, 2H), 2.94 (s, 12H), 1.70 – 1.60 (m, 2H), 1.46 – 1.36 (m, 2H), 1.36 – 1.19 (m, 4H), 0.65 (s, 3H), 0.53 (s, 3H). Analytical HPLC, > 99% purity (4.6 mm × 150 mm 5 μm C18 column; 2 μl injection; 5-100% CH_3CN/H_2O, linear-gradient, with constant 0.1% v/v TFA additive; 6 min run; 0.6 ml/min flow; ESI; positive ion mode; detection at 650 nm). HRMS (ESI) calcd for $C_{37}H_{49}ClN_3O_5Si$ $[M+H]^+$ 678.3130, found 678.3133.

Synthesis of JF646-HTL

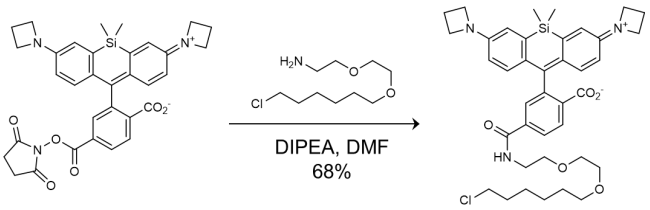

JF646-NHS Ester JF646-HTL

JF646-NHS Ester (24 mg, 40 μmol, 1.0 eq., obtained from AAT Bioquest) and HaloTag(O2)amine (13 mg, 60 μmol, 1.5 eq.) were dissolved in 2 ml anhydrous DMF. DIPEA (13 μl, 80 μmol, 2.0 eq.) was then added, and the mixture was stirred at room temperature overnight. Purification of the mixture by reverse phase-HPLC (eluent, a 30-min linear gradient, from 20% to 95% solvent B; flow rate, 5.0 ml/min; detection wavelength, 650 nm; eluent A (ddH_2O containing 0.1% TFA (v/v)) and eluent B (CH_3CN)) provided JF646-HTL (19 mg, 68% yield) as a blue solid.

^{1}H NMR ($CDCl_3$, 400 MHz) δ 8.00 (dd, *J* = 8.0, 0.7 Hz, 1H), 7.92 (dd, *J* = 8.0, 1.3 Hz, 1H), 7.70 (dd, *J* = 1.2, 0.7 Hz, 1H), 6.75 (d, *J* = 8.7 Hz, 2H), 6.73 – 6.67 (m, 1H), 6.65 (d, *J* = 2.6 Hz, 2H), 6.26 (dd, *J* = 8.8, 2.7 Hz, 2H), 3.89 (t, *J* = 7.3 Hz, 8H), 3.67 – 3.60 (m, 6H), 3.56 – 3.53 (m, 2H), 3.50 (t, *J* = 6.5 Hz, 2H), 3.39 (t, *J* = 6.6 Hz, 2H), 2.39 – 2.30 (m, 4H), 1.78 – 1.68 (m, 2H), 1.56 – 1.47 (m, 2H), 1.44 – 1.35 (m, 2H), 1.35 – 1.25 (m, 2H), 0.63 (s, 3H), 0.56 (s, 3H). Analytical HPLC, > 99% purity (4.6 mm × 150 mm 5 μm C18 column; 2 μl injection; 5-100% CH_3CN/H_2O, linear-gradient, with constant 0.1% v/v TFA additive; 6 min run; 0.6 mL/min flow; ESI; positive ion mode; detection at 650 nm). HRMS (ESI) calcd for $C_{39}H_{49}ClN_3O_5Si$ $[M+H]^+$ 702.3125, found 702.3140.

Mice and viruses

Wild-type C57BL/6J mice of both sexes (6-10 weeks of age) were obtained from Beijing Vital River Laboratory. D2R-Cre mice were kindly provided by M. Luo at the Chinese Institute for Brain Research, Beijing, and D1R-Cre mice were kindly provided by Y. Rao at Peking University. All animal protocols were approved by the Animal Care and Use Committee at Peking University. All animals were housed under a 12-h/12-h light/dark cycle at an ambient temperature of 25°C and were provided food and water ad libitum.

For dye injection in mice, unless otherwise noted, the following formulation was used: 20 μl of 5 mM SiR650 or other far-red dye (in DMF, equivalent to 100 nmol) was mixed with 20 μl Pluronic F-127 (20% w/v in DMSO, AAT Bioquest) and 100 μl PBS and injected via the tail vein the day before recording or imaging.

The following viruses were packaged at Vigene Biosciences: AAV9-hSyn-HaloDA1.0 (7.73×10^{13} viral genomes (vg)/ml), AAV9-hsyn-hChR2(H134R)-mCherry (2.53×10^{13} vg/ml), AAV9-EF1α-DIO-hChR2(H134R)-EYFP (9.12×10^{13} vg/ml), AAV9-hSyn-NE2m (1.39×10^{13} vg/ml), and AAV9-hSyn-r5-HT1.0 (1.06×10^{13} vg/ml). AAV-hsyn-haloDA1.0mut (5.38×10^{12} vg/ml) and AAV9-hsyn-DA3m (5.07×10^{12} vg/ml) were packaged at BrainVTA. In addition, the following two viruses were co-packaged at BrainVTA with mixed plasmids (1:1:1 ratio) to reduce mutual suppression: AAV9-hSyn-HaloDA1.0 / AAV9-hsyn-rACh1h / AAV9-hsyn-DIO-GFlamp2 (5.54×10^{12} vg/ml) and AAV9-hSyn-HaloDA1.0 / AAV9-hsyn-rACh1h / AAV9- hsyn-eCB2.0 (5.83×10^{12} vg/ml). AAV9-EF1α-DIO-NES-jRGECO1a (5.76×10^{12} vg/ml) was packaged at Brain Case.

Fluorescence imaging of acute brain slices

Preparation of brain slices

Adult male C57BL/6J mice (8-10 weeks old) were anesthetized via intraperitoneal injection of 2,2,2-tribromoethanol (Avertin, 500 mg/kg). A stereotaxic injection of AAV9-hSyn-HaloDA1.0 (300 nl) or a co-packaged virus containing AAV9-hSyn-HaloDA1.0, AAV9-hSyn-rACh1h, and AAV9-hSyn-eCB2.0 (400 nl total volume) was delivered into the nucleus accumbens (NAc) core at a rate of 50 nl/min. The injection coordinates were: AP +1.4 mm relative to Bregma, ML ±1.2 mm relative to Bregma, and DV -4.3 mm from the dura. After 2-4 weeks, the mice were deeply anesthetized, followed by transcardiac perfusion with cold slicing buffer consisting of (in mM): 110 choline chloride, 2.5 KCl, 1.25 NaH_2PO_4, 25 $NaHCO_3$, 7 $MgCl_2$, 25 glucose, and 0.5 $CaCl_2$. The brain was quickly extracted, placed in cold, oxygenated slicing buffer, and sectioned into 300-μm coronal slices using a VT1200 vibratome (Leica).

For imaging of JF646-labeled slices, the brain slices were first incubated in oxygenated ACSF containing 1 μM JF646 at room temperature for 60 min. The ACSF contained (in mM): 125 NaCl, 2.5 KCl, 1 NaH_2PO_4, 25 $NaHCO_3$, 1.3 $MgCl_2$, 25 glucose, and 2 $CaCl_2$. After incubation, the slices were transferred to fresh oxygenated ACSF and allowed to sit for at least 60 min to remove any non-specific dye binding. For imaging of SiR650-labeled slices, 100 nmol of SiR650 was injected into the tail vein; 12 h after injection, acute brain slices were prepared as described above and incubated in oxygenated ACSF for at least 60 min at room temperature before imaging.

Single-color imaging of acute brain slices

Confocal imaging was conducted using a Zeiss LSM-710 confocal microscope equipped with a N-Achroplan 20x (NA: 0.5) water-immersion objective, a HeNe633 laser, a HeNe543 laser, and an Argon laser. The microscope was controlled using ZEN2012, 11.0.4.190 software (Zeiss). Slices were mounted in a custom-made imaging chamber with continuous ACSF perfusion at 2 ml/min.

HaloDA1.0 labeled with JF646 was excited using a 633-nm laser, and fluorescence emission captured at 638-747 nm. Images were acquired at a size of 256 × 256 pixels and a frame rate of 5 Hz. Electrical stimuli were applied using a Grass S48 stimulator (Grass Instruments). A bipolar electrode (WE30031.0A3, MicroProbes) was placed near the NAc core under fluorescence guidance, and stimuli were applied at a voltage of 4-7 V and a pulse duration of 1 ms. Synchronization of imaging and stimulation was facilitated using an Arduino board (Uno) with custom scripts controlling the process. To calculate $\Delta F/F_0$, baseline fluorescence was defined as the average fluorescence signal obtained for 10 s before stimulation.

For kinetics measurements, a zoomed-in region (64 x 64 pixels) was scanned at a frame rate of 13.5 Hz. A single 1-ms pulse was delivered, and resulting increase and subsequent decrease in fluorescence were fitted with single-exponential functions.

Three-color imaging of acute brain slices

Three-color imaging of acute brain slices was performed using a Zeiss LSM-710 confocal microscope, with the signals from three sensor captured in two sequential scans in order to minimize spectral interference. First, we simultaneously imaged HaloDA1.0 and eCB2.0; we then

performed a separate scan to image rACh1h. HaloDA1.0 was excited at 633 nm, and the emitted fluorescence was captured at 645-700 nm; eCB2.0 was excited at 488 nm, and the emitted fluorescence was captured at 509-558 nm; finally, rACh1h was excited at 543 nm, and the emitted fluorescence was captured at 580-625 nm. Images were acquired at 256 × 256 pixels at a frequency of 4 Hz. The change in fluorescence was calculated as described above, with the baseline calculated using as the average fluorescence signal measured for 0-10 s before stimulation. Rise t_{50} is defined as the time required for the sensor fluorescence to reach half of peak fluorescence. Decay t_{50} is defined as the time required for the sensor fluorescence to decay from the peak fluorescence to half of peak fluorescence. The representative images in Fig. 2F with antagonists were averaged over 5 frames at the end of stimulation.

Field stimuli (1-ms duration) were applied using parallel platinum electrodes (1 cm apart), with voltage ranging from 40-80 V. During imaging, the following compounds were added to the imaging chamber at a rate of 2 ml/min: SCH-23390 (MedChemExpress), scopolamine (MedChemExpress), AM251 (Cayman), GBR12909 (MedChemExpress), and donepezil (MedChemExpress).

Fluorescent imaging of zebrafish larvae

For these experiments, we used 4-6 days post-fertilization (dpf) zebrafish larvae. Before imaging, the larvae were immersed in dye (3.3 μM) for 1 h, then transferred to plain water for 2 h to remove the dye from the larvae's surface. Zebrafish embryos and larvae were maintained at 28°C on a 14-h light and 10-h dark cycle. All procedures were approved by the Institute of Neuroscience, Chinese Academy of Sciences.

Comparison of various dyes in zebrafish

For single-channel imaging, the elavl3:Tet^{off}-HaloDA1.0-P2A-EGFP or elavl3:Tet^{off}-HaloDAmut-P2A-EGFP plasmid (25 ng/μl) mixed with Tol2 transposase mRNA (25 ng/μl) was injected into fertilized embryos on a Nacre (*mitfa*$^{w2/w2}$) background at the one-cell stage in order to generate chimeric transgenic fish. Positive fish were selected based on EGFP expression. After being labeled with dye, the zebrafish were embedded in 2% agarose gel and imaged using an FN1 confocal microscope (Nikon) equipped with a 16x (NA: 0.8) water-immersion objective. HaloDA1.0 and HaloDAmut were excited using a 640-nm laser, and fluorescence emissions were captured at 650-750 nm. Time-lapse images were acquired at 512 x 512 pixels at ~1.06 s per frame. PBS, either with or without 100 μM DA, was locally puffed on the larvae using a micropipette with a tip diameter of 1-2 μm, targeting the optic tectum region. The change in fluorescence was calculated as described above, with the baseline calculated using the average fluorescence signal measured for 10-50 s before puff application. The overall fluorescence intensity ratio of the far-red to green channels in the optic tectum and hindbrain was used to compare brightness between dyes. For the comparison of relative background staining, background staining and sensor-expressing regions were quantified separately, with GFP serving as a marker for sensor expression.

Three-color imaging in zebrafish

For three-color imaging, the HaloDA1.0 plasmid, which co-expresses the cardiac green fluorescent marker myl7-EGFP to facilitate the selection of positive fish, was injected into double transgenic embryos in order to generate chimeric triple transgenic larval zebrafish. Specifically, the elavl3:Tet^{off}-HaloDA1.0;myl7-EGFP plasmid (25 ng/μl) mixed with Tol2 transposase mRNA (25

ng/μl) were injected into Tg(gfap:Tet^{off}-ATP1.0);Tg(elavl3:jRGECO1a) embryos. An FV3000 confocal microscope (Olympus) equipped with a 20x (NA: 1.0) water-immersion objective was used for imaging. HaloDA1.0 was excited at 640 nm, and the emitted fluorescence was captured at 650-750 nm; jRGECO1a was excited at 561 nm, and the emitted fluorescence was captured at 570-620 nm; finally, ATP1.0 was excited at 488 nm, and the emitted fluorescence was captured 500-540 nm. Time-lapse imaging was performed using the sequential line-scanning mode in order to obtain three sensor images (512 x 512 pixels) at a frame rate of 0.5 Hz.

Electric shock was generated using an ISO-Flex stimulus isolator (A.M.P.I), controlled by a programmable Arduino board (Uno), and applied using silver-plated tweezers placed parallel to the fish. Each stimulus was applied at 40 V/cm, with a duration of 1 s and an interval of 180 s. The change in fluorescence was calculated as described above, with the baseline calculated using the average fluorescence signal measured for 0-30 s before electrical shock. The cross-correlation between each pair of signals (DA, Ca^{2+}, and/or ATP) in Fig. S7F was calculated using the *xcorr* function in MATLAB. Similar cross-correlation analysis was also applied to the three-color fiber photometry data (Fig. 4M, N).

In the PTZ imaging experiment, the baseline responses were recorded for 5 min, followed by the addition of PTZ to a final concentration of 10 mM, and imaging was continued for 0.5-1 h. To identify the peak in Fig. S7G, the Ca^{2+} peak was selected using the MATLAB *findpeaks* function with a minimum peak prominence set to one-tenth of the maximum Ca^{2+} response for each zebrafish. For adjacent peaks with an interval <70 s, only the highest peak was selected. The DA, Ca^{2+}, and ATP transients were aligned to the Ca^{2+} peak. Peaks were further selected only if the peak amplitude of ATP and DA was exceeded one-tenth of the maximum response for each zebrafish.

***In vivo* fiber photometry recording with optogenetic stimulation in mice**

Optogenetic recording in the NAc and mPFC

Adult male C57BL/6J mice (8-10 weeks old) were anesthetized, and AAV9-hsyn-HaloDA1.0, AAV9-hsyn-HaloDAmut or AAV9-hsyn-DA3m (300 nl) was injected into the NAc (AP: +1.4 mm relative to Bregma, ML: ±1.2 mm relative to Bregma, and DV: -4.0 mm from the dura) or mPFC (AP: +1.98 mm relative to Bregma, ML: ±0.3 mm relative to Bregma, and DV: -1.8 mm from the dura). Virus expressing AAV9-hsyn-hChR2(H134R)-mCherry (500 nl) was injected into the ipsilateral VTA (AP: -2.9 mm relative to Bregma, ML: ±0.6 mm relative to Bregma, and DV: -4.1 mm from the dura). An optical fiber (200-μm diameter, 0.37 NA; Inper) was implanted 0.1 mm above the virus injection site in the NAc or mPFC, and another optical fiber was implanted 0.2 mm above the virus injection site in the VTA.

At 2-3 weeks after virus injection, the mice expressing HaloDA1.0 or HaloDAmut sensors were injected with various far-red dyes; 12 h after injection, photometry recording with optogenetic stimulation was performed. The sensor signals were recorded using a customized photometry system (Thinker Tech) equipped with a 640/20-nm bandpass-filtered (Model ZET640/20x; Chroma) LED light (Cree LED) for excitation of HaloDA1.0 or HaloDAmut sensors and a 470/10-nm bandpass-filtered (Model 65-144; Edmund Optics) LED light (Cree LED) for excitation of DA3m sensor; a multi-bandpass-filtered (Model ZET405/470/555/640m; Chroma) PMT (Model H10721-210; Hamamatsu) was used to collect the signal, and an amplifier (Model C7319;

Hamamatsu) was used to convert the current output from the PMT to a voltage signal. The voltage signal was passed through a low-pass filter and then digitized using an acquisition card (National Instruments). The excitation light power at the tip of the optical fiber was 80 μW and was delivered at 20 Hz with a 10-ms pulse duration.

An external 488-nm laser (LL-Laser) was used for optogenetic stimulation and was controlled by the photometry system to allow for staggered stimulation and signal recording. The stimulation light power at the tip of the fiber was 20 mW, and 10-ms pulses were applied. Three stimulation patterns were used: stimuli were applied for 1 s, 5 s, or 10 s at 20 Hz; stimuli were applied at 5 Hz, 10 Hz, 20 Hz, or 40 Hz for 10 s; and stimuli were applied for fixed duration (1 s) and frequency (20 Hz). Where indicated, the mice received an intraperitoneal injection of SCH-23390 (8 mg/kg) or GBR12909 (20 mg/kg) in a total volume of 300-400 μl. $\Delta F/F_0$ was calculated as described above, with the baseline calculated as the average fluorescence signal measured for 15-30 s before optogenetic stimulation.

Dual-color optogenetic recording in the CeA

Adult male and female D2R-Cre mice (8-12 weeks old) were used for this experiment. A 2:1 mixture of AAV9-hSyn-HaloDA1.0 and AAV9-EF1α-DIO-NES-jRGECO1a (400 nl total volume) was injected into the CeA (AP: -1 mm relative to Bregma, ML: ±2.5 mm relative to Bregma, and DV: -4.3 mm from the dura). AAV9-EF1α-DIO-hChR2(H134R)-EYFP (400 nl) was also injected into the ipsilateral VTA (AP: -2.9 mm relative to Bregma, ML: ±0.6 mm relative to Bregma, and DV: -4.1 mm from the dura). Two optical fibers (200-μm diameter, 0.37 NA; Inper) were implanted 0.1 mm above the virus injection site in the CeA and 0.2 mm above the virus injection site in the VTA.

Three weeks after virus injection, a customized three-color photometry system (Thinker Tech) was used for photometry recording as described in the following section. The system was equipped with three LEDs, but only two LEDs were used in this experiment to excite the red fluorescent jRGECO1a sensor at 40 μW and the far-red HaloDA1.0 sensor at 80 μW. The excitation lights were delivered sequentially at 20 Hz with a 10-ms pulse duration for each. An external 473-nm laser (LL-Laser) was used for optogenetic stimulation and was controlled by the photometry system to allow for staggered stimulation and signal recording. The stimulation light power at the tip of the fiber was 20 mW, with a 10-ms duration for each pulse. The day before recording, the mice received an injection of SiR650 via the tail vein. Where indicated, the mice also received an intraperitoneal injection of eticlopride (2 mg/kg) at a total volume of 350 μl. $\Delta F/F_0$ was calculated as described above, and, the baseline was calculated as the average fluorescence signal measured for 15-30 s before optogenetic stimulation. The area under the curve (AUC) in Fig. 3O was calculated during the 0-30 s period after optogenetic stimulation, with stimulus onset defined as 0 s.

***In vivo* three-color recording in the NAc**

Adult male and female D1R-Cre mice (10-14 weeks old) were used for this experiment. A co-packaged AAV mixture containing AAV9-hSyn-HaloDA1.0, AAV9-hsyn-rACh1h, and AAV9-hsyn-DIO-GFlamp2 (600 nl total volume) was unilaterally injected into the NAc (AP: +1.4 mm relative to Bregma, ML: ±1.2 mm relative to Bregma, and DV: -4.0 mm from the dura), and an

optical fiber (200-μm diameter, 0.37 NA; Inper) was implanted 0.1 mm above the virus injection site.

Photometry recording was performed 2-3 weeks after virus injection using a customized three-color photometry system (Thinker Tech). A 470/10-nm (model 65144; Edmund optics) filtered LED at 40 μW was used to excite the green fluorescent sensors; a 555/20-nm (model ET555/20x; Chroma) filtered LED at 40 μW was used to excite the red fluorescent sensors; and a 640/20-nm (model ZET640/20x; Chroma) filtered LED at 40 μW was used to excite the far-red fluorescent sensors. The three excitation lights were delivered sequentially at 20-Hz with a 10-ms pulse duration for each, and fluorescence was collected using an sCMOS (Tucsen) and filtered with a three-bandpass filter (model ZET405/470/555/640m; Chroma). To minimize autofluorescence from the optical fiber, the recording fiber was photobleached using a high-power LED before recording. The day before recording, the mice received an injection of SiR650 via the tail vein.

Sucrose

For sucrose delivery, an intraoral cheek fistula was implanted in each mouse. In brief, incisions were made in the cheek and the scalp at the back of the neck. A short, soft silastic tube (inner diameter: 0.5 mm; outer diameter: 1 mm) connected via an L-shaped stainless-steel tube was then inserted into the cheek incision site. The steel tube was routed through the scalp incision, with the opposite end inserted into the oral cavity. After 3 d of recovery from the surgery, the mice were water-restricted for 36 h (until reaching 85% of their initial body weight). The water-restricted, freely moving mice then received 5% sucrose water delivery (approximately 8 μl per trial, with 25-50 trials per session and a trial interval of 20-30 s).

Foot shock

The mice were placed in a shock box and habituated for 30 min. During the experiment, ten 1-s pulses of electricity were delivered at 0.7 mA, with an interval of 90-120 s between trials.

Cocaine

Cocaine HCl was obtained from the Qinghai Pharmaceutical Factory and dissolved in 0.9% saline. The mice received an intraperitoneal injection of cocaine (20 mg/kg) in a total volume of 300-400 μl. Photometry signals were recorded for 10-15 min before and 60 min after cocaine injection. The signals were low-pass filtered (0.01 Hz) to remove spontaneous fluctuations in fluorescence.

Data analysis of three-color photometry

The photometry data were analyzed using a custom program written in MATLAB. For the sucrose experiment, the baseline was defined as the average fluorescence signal measured for 3-6 s before sucrose delivery; for the foot shock experiment, the baseline was defined as the average fluorescence signal measured for 0-3 s before foot shock delivery; for the cocaine experiment, the baseline was defined as the average fluorescence signal measured for 0-600 s before cocaine injection. To quantify the change in fluorescence across multiple animals, $\Delta F/F_0$ was normalized using the standard deviation of the baseline signals in order to obtain a *Z*-score.

Signals recorded between adjacent sucrose deliveries (10 s after one sucrose delivery and 5 s before the next sucrose delivery) were used to analyze spontaneous activity (as shown in Fig. 4E, I). The DA peaks were identified using the MATLAB *findpeaks* function, with a minimum peak

prominence of 2x the standard deviation; standard deviation was calculated based on the baseline following SCH administration. The DA, ACh, and cAMP transients were aligned to the DA peak.

Measurement of dye labeling percentage

Adult male wild-type mice (7-8 weeks old) were used for this experiment. AAV9-hSyn-HaloDA1.0 (diluted to 5×10^{12} vg/ml, 300nL) was injected into the NAc (AP: +1.4 mm relative to Bregma, ML: ±1.2 mm relative to Bregma, and DV: -4.0 mm from the dura). At 2-3 weeks after virus injection. Mice was tail-vein injected with 100 nmol of one of the far-red dyes (JF635, JF646, SiR650, or JFX646). After 12 h, acute brain slices were prepared following the protocol described in the "preparation of brain slices" section. All acute brain slices containing the NAc brain area (approximately 5 slices, 300-μm thickness per slice) were collected and homogenized using a motorized tissue grinder (Tissuelyser) in 1 mL PBS (pH 7.4) with protease inhibitors (Roche, 04693132001).

The homogenates of each sample were evenly divided into two portions and centrifuged at 12000 rpm at 4 ℃ for 3 min. For the pellets of each sample, one portion was resuspended with 5 μM JF525 (in PBS) to fully label any HaloDA1.0 sensors that were not labeled by the far-red dye, while the other portion was resuspended in PBS as a control. Both portions were incubated at room temperature for 2 h on a rotator. After incubation, all samples were centrifuged at 12000 rpm at 4 ℃ for 3 min, and the pellet was collected and resuspended in PBS, repeating this step for 3 times. The pellets were then resuspended in a lysis buffer containing home-purified PNGaseF at a concentration of $A280_{sample} : A280_{PNGaseF} = 10 : 1$, 1% n-Dodecyl-β-D-Maltopyranoside (DDM; MREDA), and protease inhibitors (Roche, 04693132001). The samples were incubated at 4 ℃ for 1 h on a rotator for thorough lysis. The lysates were then centrifuged at 40000 rpm at 4 ℃ for 30 min, and the supernatant was mixed with SDS loading buffer. 20 μL of each sample was loaded per lane, and Sodium dodecyl-sulfate polyacrylamide gel electrophoresis (SDS-PAGE, 10%) was performed at 200 V and 4 ℃ for 60 min. Images were acquired using a ChemiDoc MP system (Bio-Rad Laboratories). JF525-labeled samples were excited by 512/25 nm, and fluorescence was collected at 535/25 nm; far-red dye-labeled samples were excited by 635/25 nm, and fluorescence was collected at 700/50 nm.

For HEK293T samples, HEK293T cells expressing HaloDA1.0 were collected and centrifuged at 600 g for 5 min. The cell pellet was resuspended in PBS containing protease inhibitors and evenly divided into 11 portions: 1 for blank control and the other 10 portions for incubation with 5 different dyes (JF525, JF635, JF646, SiR650, and JFX650) at either 1 μM or 10 μM concentration at room temperature for 2 h, respectively, to support full labeling at both dye concentration. The subsequent processes were the same as those for the brain slice samples.

For the calculation of far-red dye labeling percentage (P) *in vivo*, the following equations can be used:

$$\frac{sF_{FR} \cdot N \cdot P}{sF_G \cdot N \cdot (1-P)} = R_{brain\ tissues} \qquad Eq.1$$

In Eq.1, sF_{FR} and sF_G indicate the single-molecule brightness of far-red dyes and JF525, respectively; N indicates the number of expressed HaloDA1.0 molecules in the brain; $R_{brain\ tissues}$ is the fluorescent intensity ratio of the far-red channel to the green channel for the brain tissue sample on the same lane.

For cultured cell samples, where the number of HaloDA1.0 molecules labeled with each dye is the same, and supposed to be fully saturated labeled, thus the ratio of sF_{FR} to sF_G can be obtained using the equation:

$$\frac{sF_{FR} \cdot n}{sF_G \cdot n} = R_{cultured\ cells} \qquad Eq.2$$

In Eq.2, *n* indicates the number of expressed HaloDA1.0 molecules in cultured HEK293T cells for each group; $R_{cultured\ cells}$ is the fluorescent intensity ratio of far-red channel for far-red-labeled cell samples to green channel for JF525-labeled cell samples.

By combining Eqs.1 and 2, the far-red dye labeling percentage (*P*) *in vivo* can be determined:

$$P = \frac{R_{brain\ tissues}}{R_{cultured\ cells} + R_{brain\ tissues}} \qquad Eq.3$$

Brightness comparison of HaloDA1.0-SiR650 to fluorescent proteins

In zebrafish

To evaluate the relative brightness of HaloDA1.0 versus fluorescent proteins in zebrafish, we measured the fluorescent intensity of zebrafish expressing D1R-EGFP (EGFP fused to the C-terminus of D1R) and SiR650-labeled HaloDA1.0, using P2A-BFP as a reference to control expression variability. To calibrate fluorescent intensity captured in different imaging channels, we performed calibration measurements using SiR650-labeled D1R-HaloTag and D1R-EGFP expressed in cultured cells, whose brightness values (extinction coefficient times quantum yield) have been previously reported. After determining the brightness of HaloDA1.0 relative to EGFP, we further compared its brightness with that of several red and far-red fluorescent proteins in the far-red spectral range (>650 nm). The relative brightness of these fluorescent proteins was estimated from the brightness and spectral data available in FPbase.

In mice

In mice, the *in vivo* brightness of HaloDA1.0-SiR650 is primarily determined by the *in vivo* labeling percentage of SiR650, which is approximately 11% (measured in Fig. S9). We first quantified the fluorescence intensity of HaloDA1.0-SiR650 relative to D1R-EGFP in cultured cells and then applied the *in vivo* labeling efficiency to estimate the *in vivo* brightness. The brightness of HaloDA1.0-SiR650 was then compared to that of red and far-red fluorescent proteins in a manner similar to the zebrafish analysis.

Immunohistochemistry

Mice were anesthetized and intracardially perfused with PBS followed by 4% paraformaldehyde (PFA) in PBS buffer. The brains were dissected and fixed overnight at 4°C in 4% PFA in PBS. The brains were then dehydrated in 30% sucrose in PBS and sectioned at a thickness of 40 μm using a cryostat microtome (CM1950; Leica). The slices were placed in blocking solution containing 5% (v/v) normal goat serum, 0.1% Triton X-100, and 2 mM $MgCl_2$ in PBS for 1 h at room temperature. The slices were then incubated in AGT solution (0.5% normal goat serum, 0.1% Triton X-100, and 2 mM $MgCl_2$ in PBS) containing primary antibodies overnight at 4°C. The following day, the slices were rinsed three times in AGT solution and incubated for 2 h at room temperature with secondary antibodies containing DAPI (5 mg/ml, dilution 1:1,000; catalog no. HY-D0814, MedChemExpress). After three washes in AGT solution, the slices were mounted on

slides and imaged using a VS120-S6-W Virtual Slide Microscope (Olympus) equipped with a 10× (NA: 0.4) objective.

Anti-HaloTag primary antibody (rabbit, 1 mg/ml, dilution 1:500; catalog no. G928A, Promega) and iFluor 647-conjugated anti-rabbit secondary antibody (goat, 1 mg/ml, dilution 1:500; catalog no. 16837, AAT Bioquest) were used for HaloDA1.0 and HaloDAmut. Anti-mCherry primary antibody (mouse, 1 mg/ml, dilution 1:1000; catalog no. ab125096, Abcam) and iFluor 555-conjugated anti-mouse secondary antibody (goat, 1 mg/ml, dilution 1:500; catalog no. 16776, AAT Bioquest) were used for jRGECO1a, rACh1h, and ChR2-mcherry. Anti-GFP antibody (chicken, 10 mg/ml, dilution 1:500; catalog no. ab13970, Abcam) and Alexa Fluor 488-conjugated anti-chicken secondary antibody (goat, 2 mg/ml, dilution 1:500; catalog no. ab150169, Abcam) were used for GFlamp2 and ChR2-EYFP.

Quantification and statistical analysis

Imaging data were processed using ImageJ software (NIH) and custom-written MATLAB (R2020b) programs. Data were plotted using OriginPro 2020b (OriginLab) or Adobe Illustrator CC. The signal-to-noise ratio (SNR) was calculated as the peak response divided by the standard deviation of the baseline fluorescence. Except where indicated otherwise, all summary data are presented as the mean ± s.e.m. All data were assumed to be distributed normally, and equal variances were formally tested. Differences were analyzed using a two-tailed Student's *t*-test or one-way ANOVA; where applicable, $*P < 0.05$, $**P < 0.01$, $***P < 0.001$, and n.s., not significant ($P \geq 0.05$).

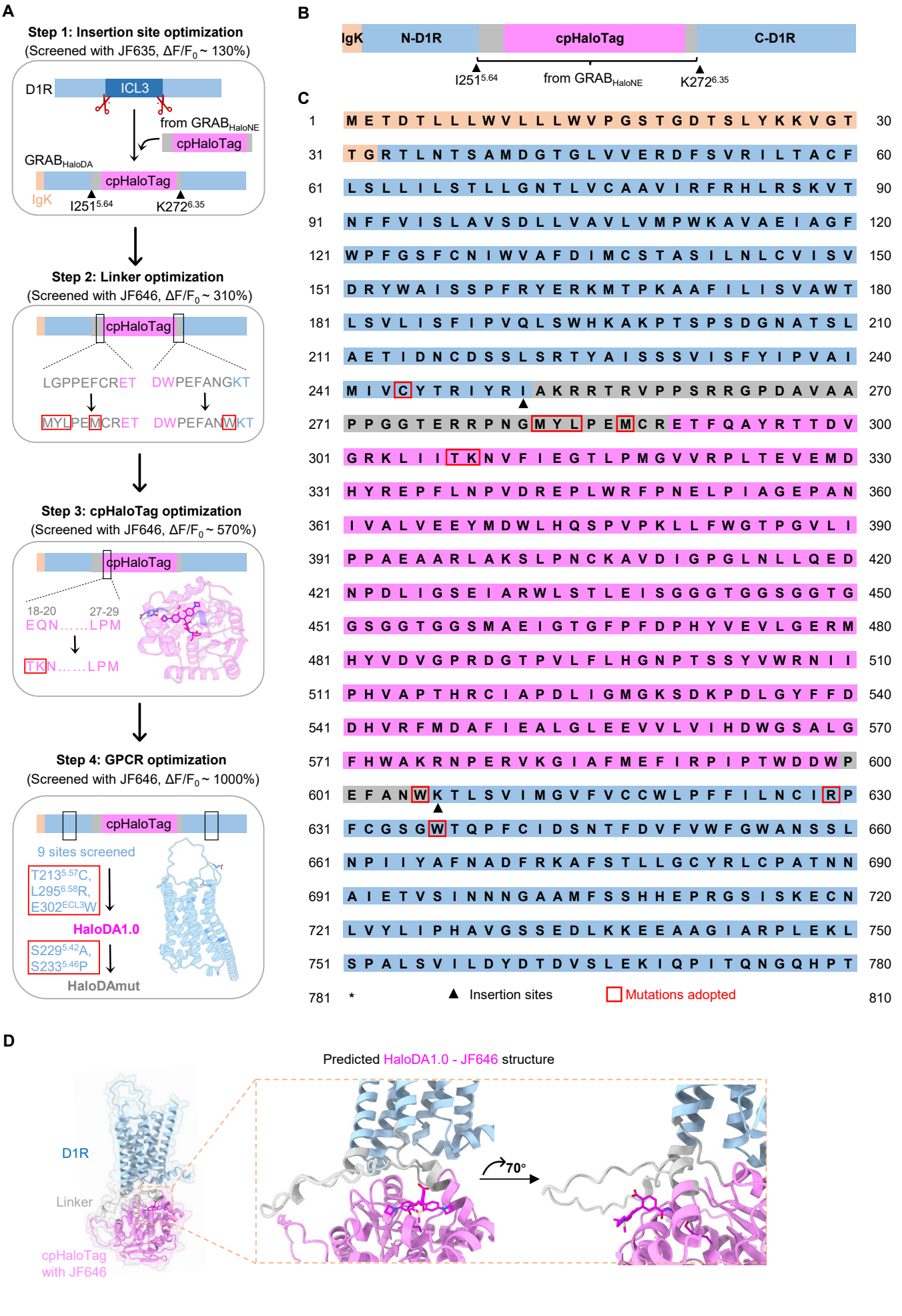
A
Step 1: Insertion site optimization
(Screened with JF635, ΔF/F0 ~ 130%)
D1R
ICL3
from GRABHaloNE
cpHaloTag
GRABHaloDA
cpHaloTag
IgK
I251 5.64
K272 6.35
Step 2: Linker optimization
(Screened with JF646, ΔF/F0 ~ 310%)
cpHaloTag
LGPPEFCRET
DWPEFANGKT
MYLPEMCRET
DWPEFANWKT
Step 3: cpHaloTag optimization
(Screened with JF646, ΔF/F0 ~ 570%)
cpHaloTag
18-20
27-29
EQN.....LPM
TKN.....LPM
Step 4: GPCR optimization
(Screened with JF646, ΔF/F0 ~ 1000%)
cpHaloTag
9 sites screened
T213 5.57C,
L295 6.58R,
E302 ECL3W
HaloDA1.0
S229 5.42A,
S233 5.46P
HaloDAmut
B
IgK
N-D1R
cpHaloTag
C-D1R
I251 5.64
from GRABHaloNE
K272 6.35
C
1 M E T D T L L L W V L L L W V P G S T G D T S L Y K K V G T 30
31 T G R T L N T S A M D G T G L V V E R D F S V R I L T A C F 60
61 L S L L I L S T L L G N T L V C A A V I R F R H L R S K V T 90
91 N F F V I S L A V S D L L V A V L V M P W K A V A E I A G F 120
121 W P F G S F C N I W V A F D I M C S T A S I L N L C V I S V 150
151 D R Y W A I S S P F R Y E R K M T P K A A F I L I S V A W T 180
181 L S V L I S F I P V Q L S W H K A K P T S P S D G N A T S L 210
211 A E T I D N C D S S L S R T Y A I S S S V I S F Y I P V A I 240
241 M I V C Y T R I Y R I A K R R T R V P P S R R G P D A V A A 270
271 P P G G T E R R P N G M Y L P E M C R E T F Q A Y R T T D V 300
301 G R K L I I T K N V F I E G T L P M G V V R P L T E V E M D 330
331 H Y R E P F L N P V D R E P L W R F P N E L P I A G E P A N 360
361 I V A L V E E Y M D W L H Q S P V P K L L F W G T P G V L I 390
391 P P A E A A R L A K S L P N C K A V D I G P G L N L L Q E D 420
421 N P D L I G S E I A R W L S T L E I S G G G T G G S G G T G 450
451 G S G G T G G S M A E I G T G F P F D P H Y V E V L G E R M 480
481 H Y V D V G P R D G T P V L F L H G N P T S S Y V W R N I I 510
511 P H V A P T H R C I A P D L I G M G K S D K P D L G Y F F D 540
541 D H V R F M D A F I E A L G L E E V V L V I H D W G S A L G 570
571 F H W A K R N P E R V K G I A F M E F I R P I P T W D D W P 600
601 E F A N W K T L S V I M G V F V C C W L P F F I L N C I R P 630
631 F C G S G W T Q P F C I D S N T F D V F V W F G W A N S S L 660
661 N P I I Y A F N A D F R K A F S T L L G C Y R L C P A T N N 690
691 A I E T V S I N N N G A A M F S S H H E P R G S I S K E C N 720
721 L V Y L I P H A V G S S E D L K K E E A A G I A R P L E K L 750
751 S P A L S V I L D Y D T D V S L E K I Q P I T Q N G Q H P T 780
781 * ▲ Insertion sites Mutations adopted 810
D
Predicted HaloDA1.0 - JF646 structure
D1R
Linker
cpHaloTag
with JF646
70°

Fig. S1. Strategy for optimizing the HaloDA sensors.
(**A**) Schematic diagram showing the design and optimization of HaloDA1.0 and HaloDAmut. The structure in step 3 is from the resolved cpHaloTag structure (PDB: 6U2M); the structure in step 4 is from the resolved D1R structure (PDB: 7JVQ). IgK refers to the IgK leader sequence.
(**B** and **C**) Schematic depiction (**B**) and amino acid sequence (**C**) of HaloDA1.0; the black triangles indicate the insertion sites of cpHaloTag with linkers into D1R, and the red boxes indicate mutation sites introduced during sensor optimization.
(**D**) Predicted structure of HaloDA1.0 using AlphaFold 3(*80*). JF646 conjugated with the HaloTag ligand was docked into the structure by alignment with the published cpHaloTag-dye structure (PDB: 6U2M).

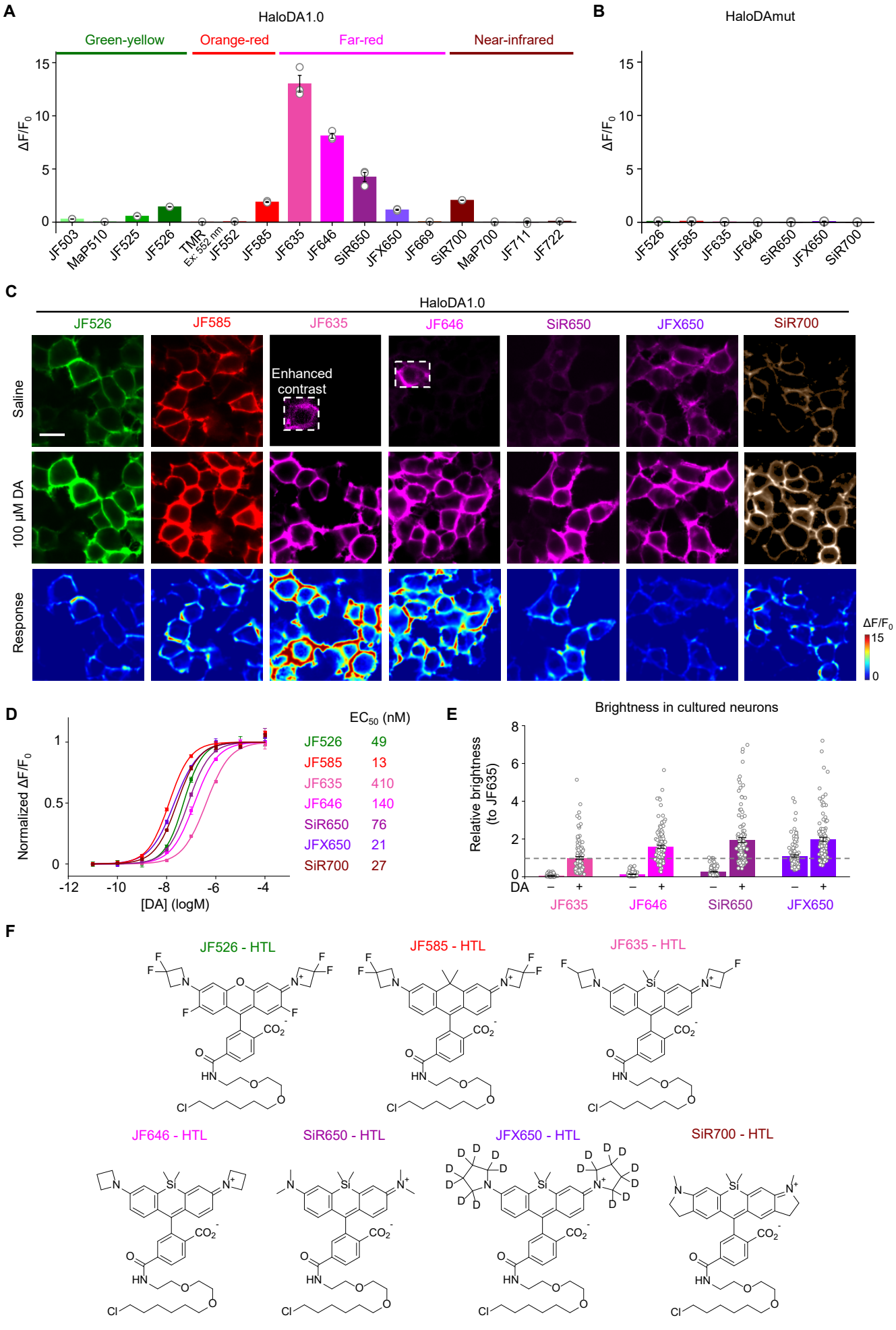
A
HaloDA1.0
Green-yellow
Orange-red
Far-red
Near-infrared
ΔF/F0
JF503
MaP510
JF525
JF526
TMR Ex. 552 nm
JF552
JF585
JF635
JF646
SiR650
JFX650
JF669
SiR700
MaP700
JF711
JF722
B
HaloDAmut
JF526
JF585
JF635
JF646
SiR650
JFX650
SiR700
C
HaloDA1.0
Saline
100 μM DA
Response
Enhanced contrast
ΔF/F0
D
Normalized ΔF/F0
[DA] (logM)
EC50 (nM)
JF526 49
JF585 13
JF635 410
JF646 140
SiR650 76
JFX650 21
SiR700 27
E
Brightness in cultured neurons
Relative brightness (to JF635)
DA
JF635
JF646
SiR650
JFX650
F
JF526 - HTL
JF585 - HTL
JF635 - HTL
JF646 - HTL
SiR650 - HTL
JFX650 - HTL
SiR700 - HTL

Fig. S2. Performance of HaloDA1.0 sensors labeled with various dyes.
(**A** and **B**) Maximum $\Delta F/F_0$ of HaloDA1.0 (**A**) and HaloDAmut (**B**) expressed in HEK293T cells and labeled with the indicated dyes; n = 3 wells with 300–500 cells per well.
(**C**) Representative images of HEK293T cells expressing HaloDA1.0 and labeled with the indicated dyes before and after application of 100 μM DA. Scale bar, 20 μm.
(**D**) Normalized dose-response curves of HaloDA1.0 expressed in HEK293T cells and labeled with the indicated dyes; n = 3 wells with 300–500 cells per well.
(**E**) Relative brightness (normalized to JF635-labeled HaloDA1.0 measured in the presence DA) of HaloDA1.0 expressed cultured rat cortical neurons expressing HaloDA1.0 and labeled with the indicated dyes; n = 120 regions of interest (ROIs) from 4 coverslips for each dye.
(**F**) Structures of the indicated seven dyes conjugated with the HaloTag ligand (HTL).

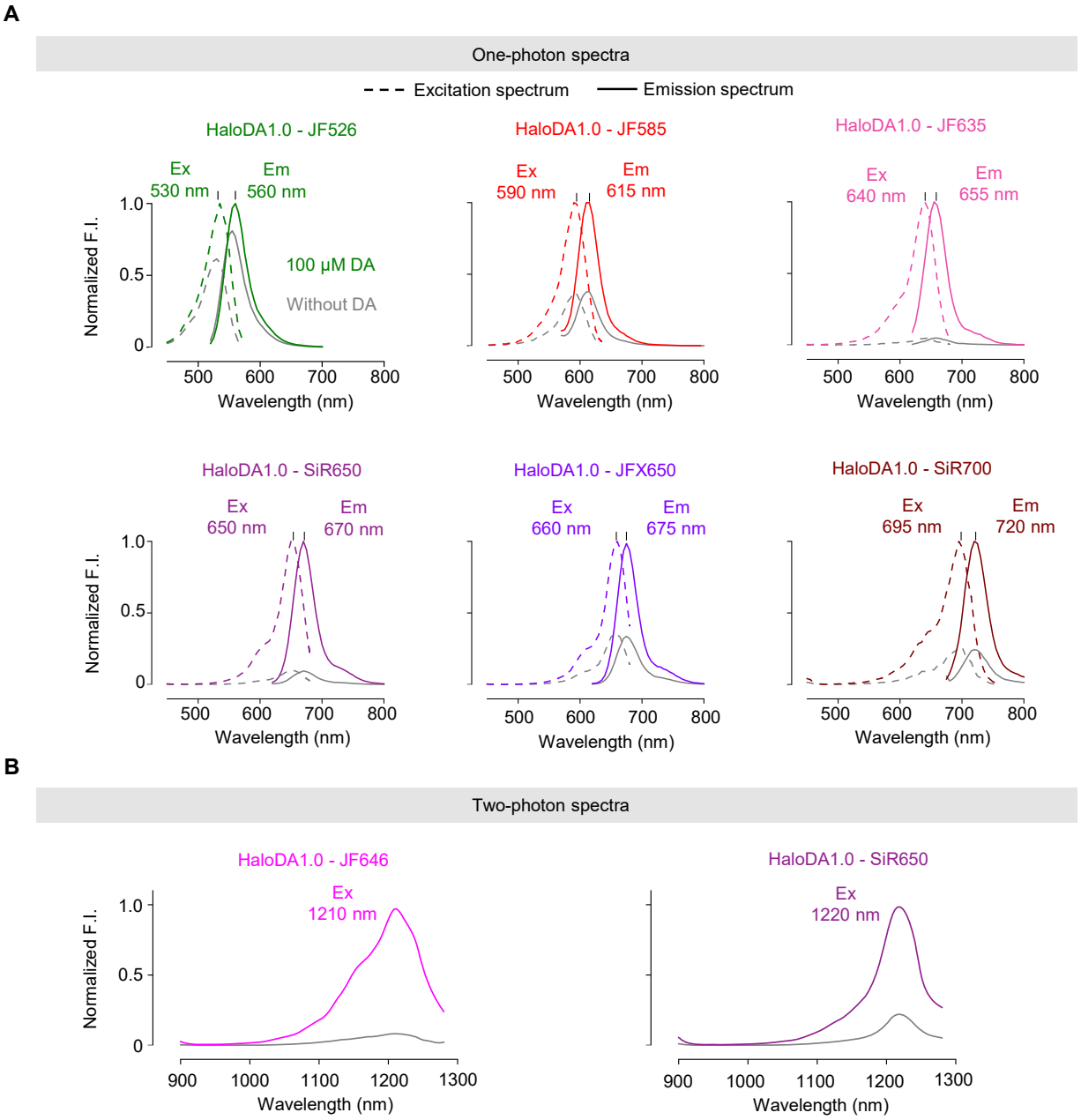

Fig. S3. Spectral properties of HaloDA1.0 sensors labeled with various dyes.
(**A**) One-photon excitation (Ex, dash line) and emission (Em, solid line) spectra of HaloDA1.0 labeled with the indicated dyes and measured in the absence (gray line) and presence of 100 μM DA (colored line).
(**B**) Two-photon excitation and emission spectra of HaloDA1.0 labeled with the indicated dyes and measured in the absence (gray line) and presence of 100 μM DA (colored line).

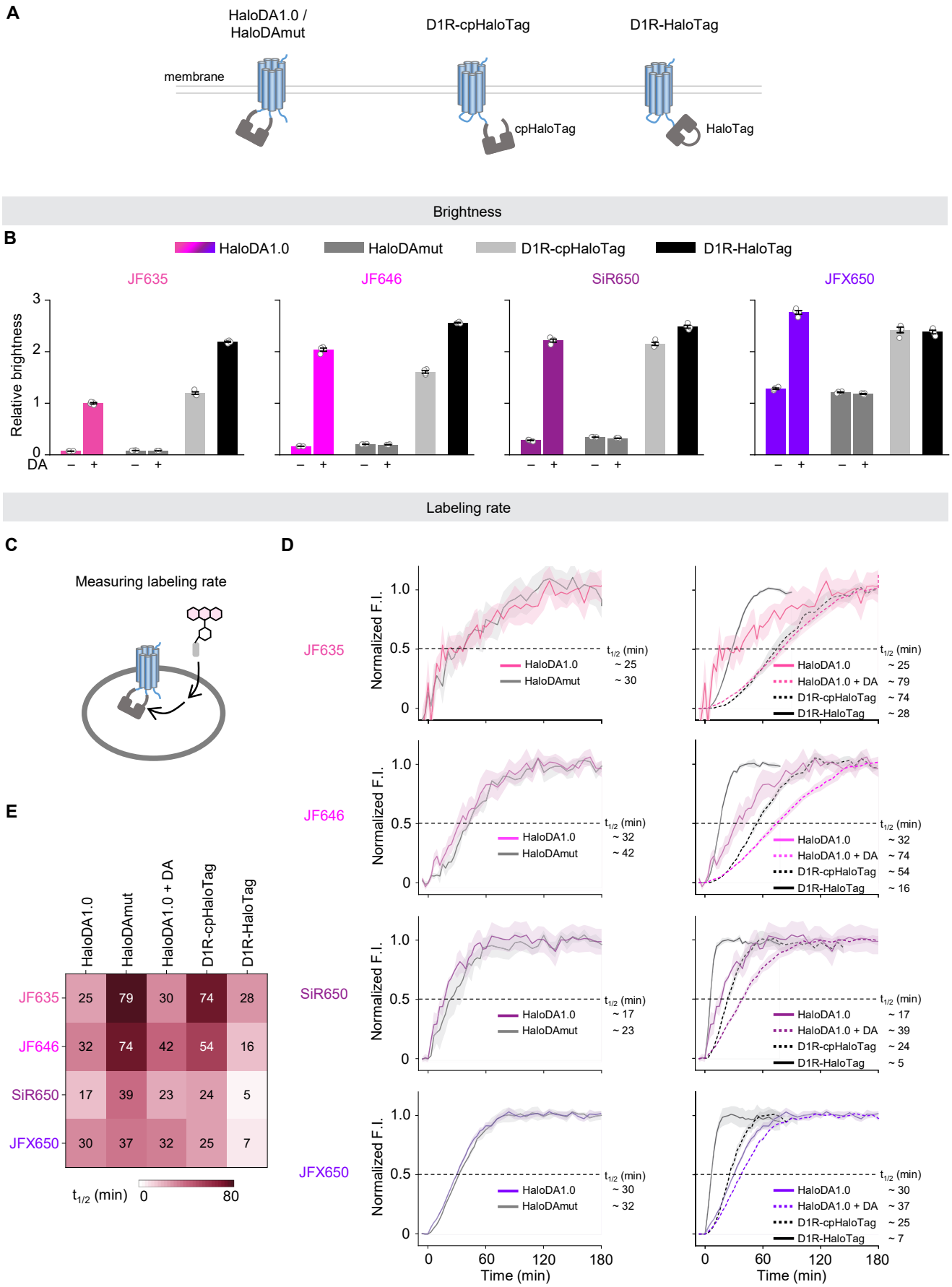
A
HaloDA1.0 / HaloDAmut
D1R-cpHaloTag
D1R-HaloTag
membrane
cpHaloTag
HaloTag
Brightness
B
HaloDA1.0
HaloDAmut
D1R-cpHaloTag
D1R-HaloTag
JF635
JF646
SiR650
JFX650
Relative brightness
DA
C
Measuring labeling rate
D
Normalized F.I.
Time (min)
t1/2 (min)
HaloDA1.0
HaloDAmut
HaloDA1.0 + DA
D1R-cpHaloTag
D1R-HaloTag
~ 25
~ 30
~ 79
~ 74
~ 28
~ 32
~ 42
~ 54
~ 16
~ 17
~ 23
~ 39
~ 24
~ 5
~ 37
~ 7
E
HaloDA1.0
HaloDAmut
HaloDA1.0 + DA
D1R-cpHaloTag
D1R-HaloTag
JF635 25 79 30 74 28
JF646 32 74 42 54 16
SiR650 17 39 23 24 5
JFX650 30 37 32 25 7
t1/2 (min) 0 80
Labeling rate

Fig. S4. Brightness and labeling rate of HaloDA1.0 sensors in cultured cells.
(**A**) Schematic diagram of HaloDA1.0, HaloDA1.0-mut, D1R-cpHaloTag and D1R-HaloTag.
(**B**) Relative brightness (normalized to JF635-labeled HaloDA1.0 measured in the presence DA) of HaloDA1.0, HaloDA1.0-mut, D1R-cpHaloTag and D1R-HaloTag expressed in HEK293T cells and labeled with the indicated dyes; n = 4 wells with 300–500 cells per well.
(**C** to **E**) Schematic diagram (**C**), fluorescent traces (**D**) and group summary (**E**) of labeling rate of HaloDA1.0, HaloDA1.0-mut, D1R-cpHaloTag and D1R-HaloTag expressed in HEK293T cells in the presence of 1 μM of indicated dyes. n = 3 wells with 100–200 cells per well.

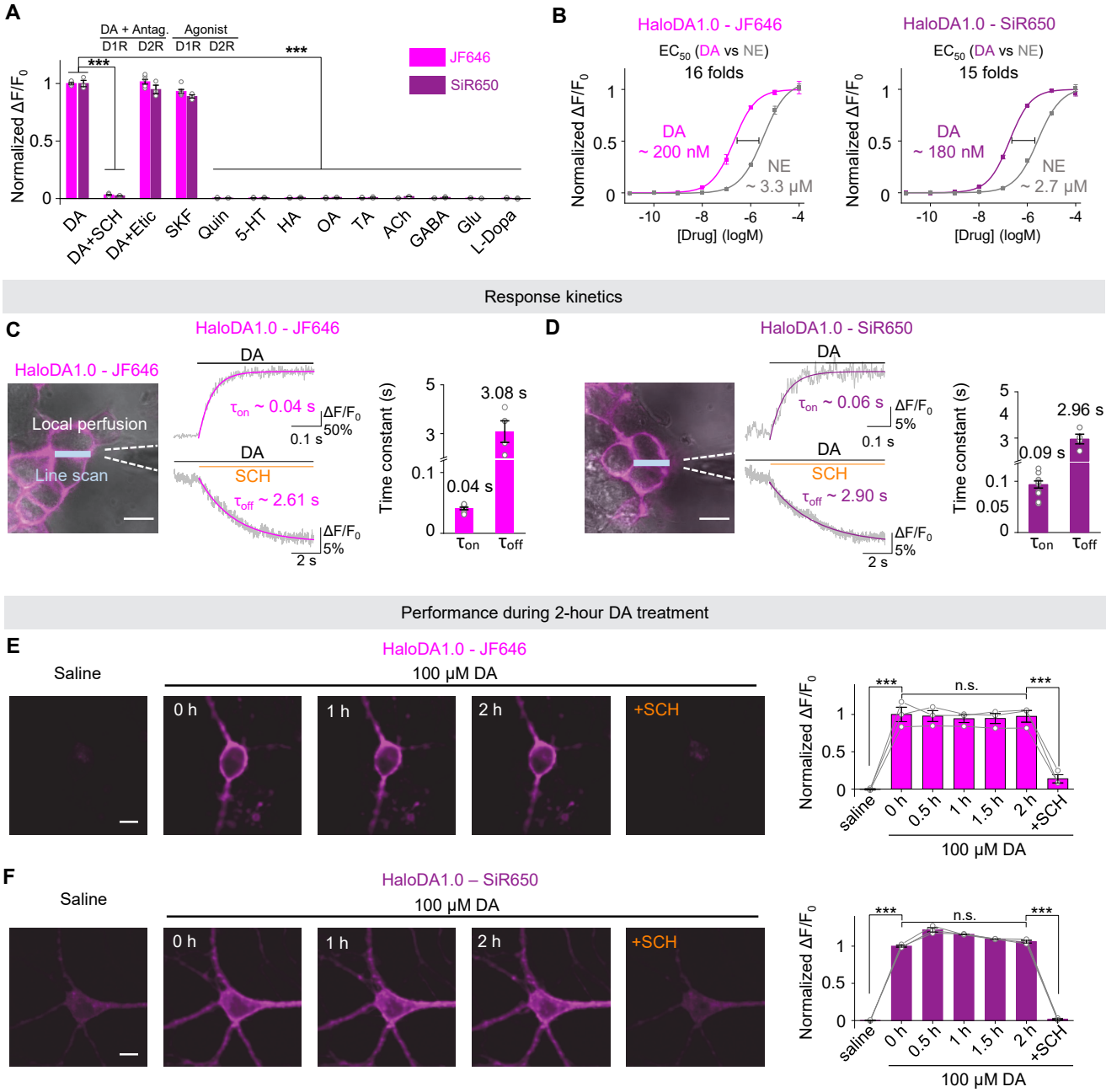
Pharmacological profiles in HEK293T
A
DA + Antag.
Agonist
D1R D2R D1R D2R
***
***
JF646
SiR650
Normalized ΔF/F0
DA
DA+SCH
DA+Etic
SKF
Quin
5-HT
HA
OA
TA
ACh
GABA
Glu
L-Dopa
B
HaloDA1.0 - JF646
EC50 (DA vs NE)
16 folds
DA
~ 200 nM
NE
~ 3.3 μM
[Drug] (logM)
HaloDA1.0 - SiR650
EC50 (DA vs NE)
15 folds
DA
~ 180 nM
NE
~ 2.7 μM
[Drug] (logM)
Response kinetics
C
HaloDA1.0 - JF646
Local perfusion
Line scan
DA
τon ~ 0.04 s
ΔF/F0
50%
0.1 s
DA
SCH
τoff ~ 2.61 s
ΔF/F0
5%
2 s
Time constant (s)
3.08 s
0.04 s
τon
τoff
D
HaloDA1.0 - SiR650
DA
τon ~ 0.06 s
ΔF/F0
5%
0.1 s
DA
SCH
τoff ~ 2.90 s
ΔF/F0
5%
2 s
Time constant (s)
2.96 s
0.09 s
τon
τoff
Performance during 2-hour DA treatment
E
HaloDA1.0 - JF646
Saline
100 μM DA
0 h
1 h
2 h
+SCH
Normalized ΔF/F0
***
n.s.
***
saline
0 h
0.5 h
1 h
1.5 h
2 h
+SCH
100 μM DA
F
HaloDA1.0 – SiR650
Saline
100 μM DA
0 h
1 h
2 h
+SCH
Normalized ΔF/F0
***
n.s.
***
saline
0 h
0.5 h
1 h
1.5 h
2 h
+SCH
100 μM DA

Fig. S5. Characterization of the HaloDA1.0 sensors expressed in cultured cells.
(**A**) Summary of the response of HaloDA1.0 expressed in cultured HEK293T cells and labeled with JF646 or SiR650. All chemicals were applied at 1 μM; n = 3 wells for each condition.
(**B**) Dose-response curves of HaloDA1.0 expressed in cultured HEK293T and labeled with JF646 (left) or SiR650 (right), in response to DA or NE; n = 3 wells for each condition.
(**C** and **D**) Schematic illustration (left), representative traces (middle), and group summary (right) of the response to locally puffing DA or SCH in order to measure the kinetics of HaloDA1.0 labeled with JF646 (**C**) or SiR650 (**D**). τ_{on} was measured following a puff of DA, while τ_{off} was measured following a puff of SCH in the presence of DA; n = 4–9 cells each. Each trace was fitted with a single-exponential function. Scale bars, 20 μm.
(**E** and **F**) Representative images (left) and group summary of normalized $\Delta F/F_0$ (right) measured in cultured neurons expressing HaloDA1.0 and labeled with JF646 (**E**) or SiR650 (**F**) before and up to 2 hours after application of 100 μM DA, followed by the addition of 100 μM SCH; n = 3 coverslips for each condition. Scale bars, 10 μm.

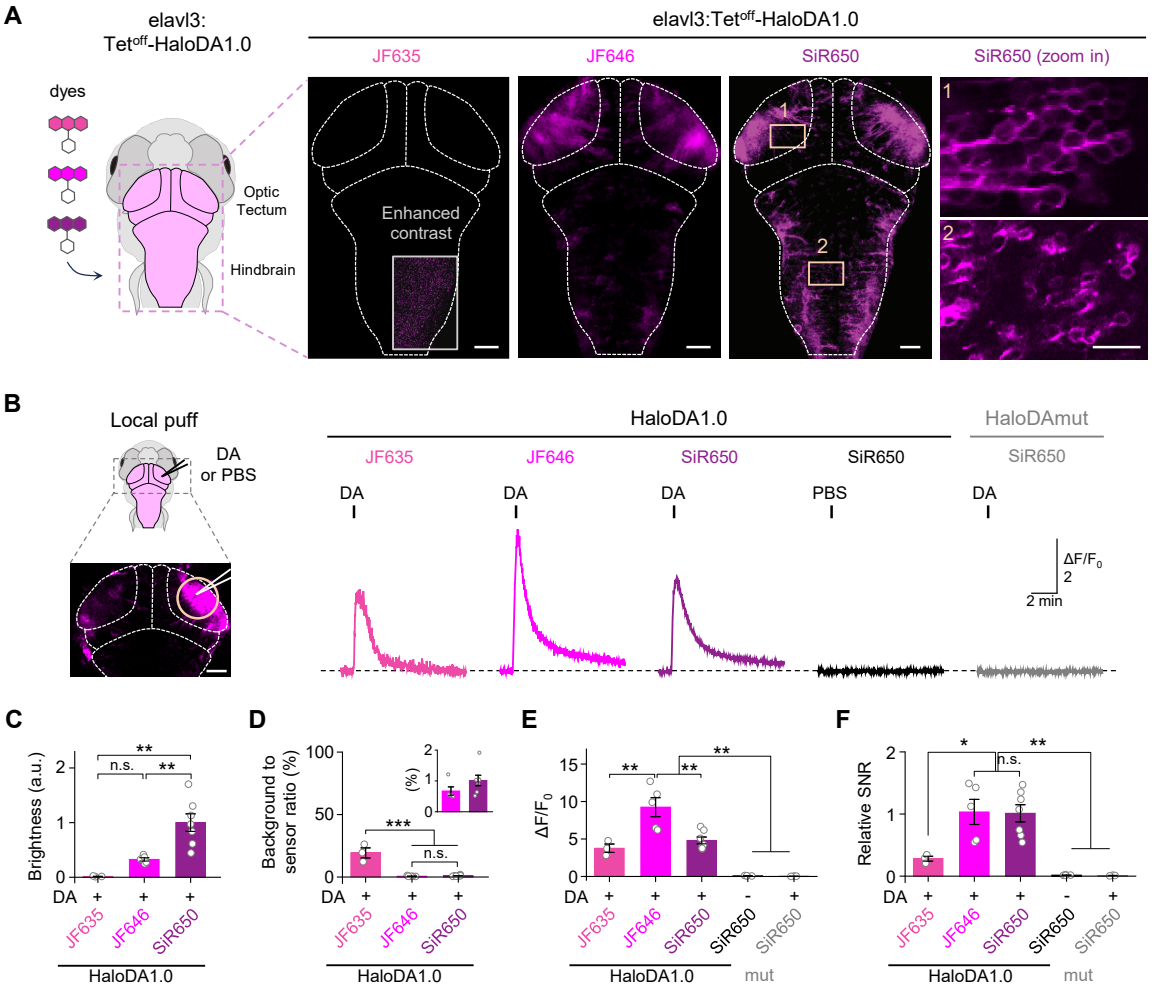

Fig. S6. Performance of HaloDA1.0 sensors in zebrafish labeled with various dyes.
(**A**) (Left) Schematic diagram of the zebrafish larvae's head with various dye labeling and the indicated field of view for confocal imaging. (Right) Representative images of the expression of HaloDA1.0 labeled with JF635, JF646, or SiR650. Scale bars, 50 μm. Two expanded views showing single-cell resolution in the indicated brain regions in SiR650-labeled zebrafish are shown on the right (scale bar, 20 μm).
(**B**) (Left) Schematic diagram and representative image of a local puff of DA or PBS onto the zebrafish brain. The orange circle (100 μm diameter) indicates the ROI used for further analysis. Scale bar, 50 μm. (Right) Representative traces of the change in HaloDA1.0 or HaloDAmut fluorescence measured under the indicated conditions. The short vertical black lines indicate local puffs.
(**C** to **F**) Group summary of the brightness (**C**), background staining to sensor signal ratio (**D**), $\Delta F/F_0$ (**E**), and relative SNR (**F**) in response to local puff under the indicated conditions. The inset in the **D** shows a zoomed-in view of background staining to sensor signal ratio for JF646 and SiR650-labeled HaloDA1.0. n = 3–7 zebrafish per group.

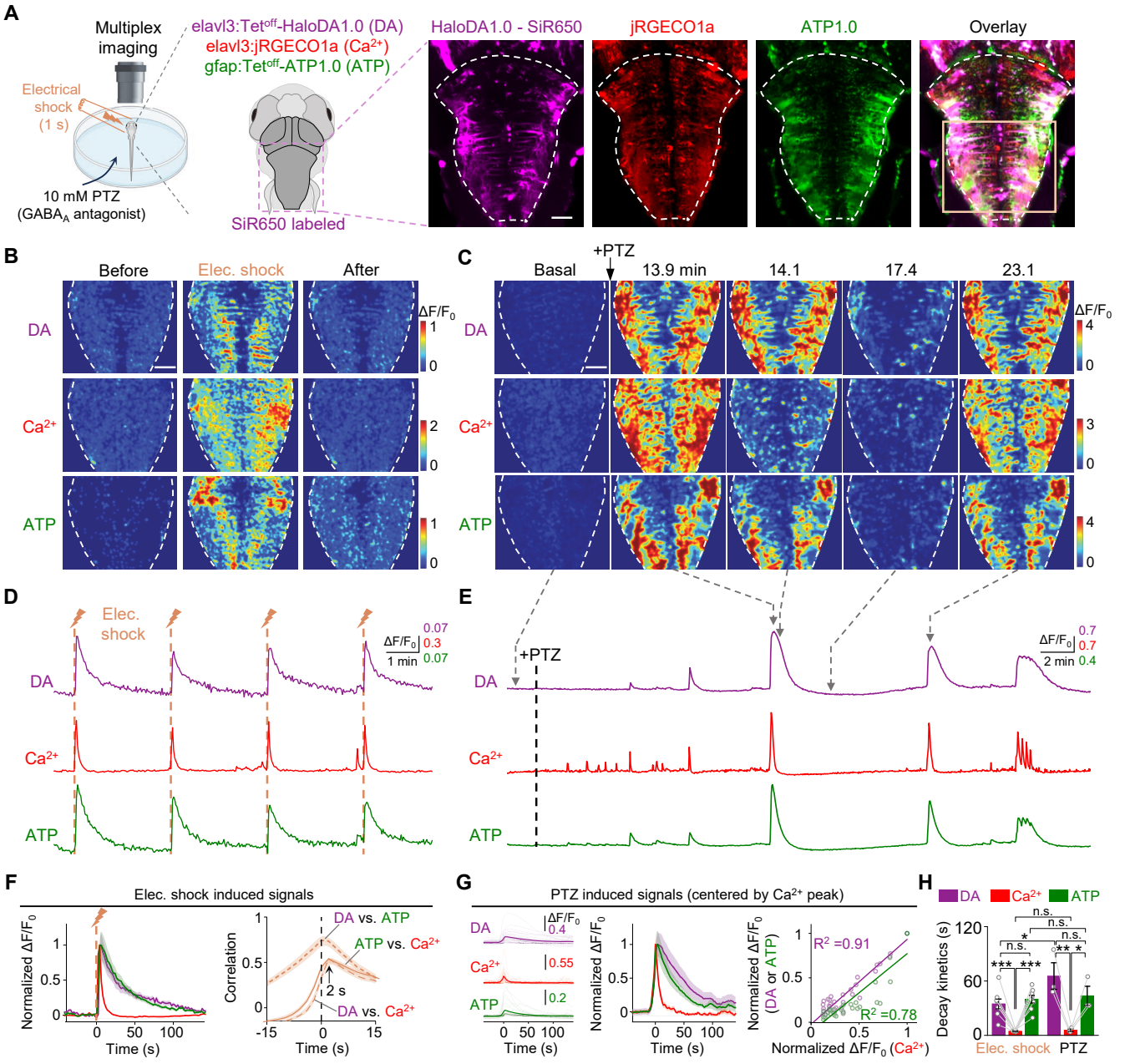
A
Multiplex imaging
Electrical shock (1 s)
10 mM PTZ (GABA$_A$ antagonist)
elavl3:Tet^{off}-HaloDA1.0 (DA)
elavl3:jRGECO1a (Ca^{2+})
gfap:Tet^{off}-ATP1.0 (ATP)
SiR650 labeled
HaloDA1.0 - SiR650
jRGECO1a
ATP1.0
Overlay
B
Before
Elec. shock
After
DA
Ca^{2+}
ATP
ΔF/F$_0$
C
Basal
+PTZ
13.9 min
14.1
17.4
23.1
D
Elec. shock
1 min
E
+PTZ
2 min
F
Elec. shock induced signals
Normalized ΔF/F$_0$
Time (s)
Correlation
DA vs. ATP
ATP vs. Ca^{2+}
DA vs. Ca^{2+}
2 s
G
PTZ induced signals (centered by Ca^{2+} peak)
R^2 =0.91
R^2 =0.78
Normalized ΔF/F$_0$ (Ca^{2+})
H
Decay kinetics (s)
n.s.
Elec. shock
PTZ

Fig. S7. Multiplex imaging in zebrafish.
(**A**) Schematic diagram and representative images of multiplex imaging in the hindbrain of zebrafish in response to a 1-s electrical shock or 10 mM pentylenetetrazole (PTZ) application. The zebrafish were labeled with SiR650. The orange box in the overlay indicates the ROI used for further analysis. Scale bar, 50 μm.
(**B** and **C**) Pseudocolor images of DA, Ca^{2+}, and ATP signals measured during electrical shock **(B)** and PTZ application **(C)**. Scale bars, 50 μm.
(**D** and **E**) Example traces of DA, Ca^{2+}, and ATP signals measured during electrical shock **(D)** and PTZ application **(E)**.
(**F**) Normalized fluorescence response (left) and cross-correlation (right) of the indicated pairs of sensor signals measured during electrical shock; n = 8 zebrafish.
(**G**) DA, Ca^{2+}, and ATP signals measured during PTZ application. (Left) Peak fluorescence responses obtained by centering all three sensor signals with the peak Ca^{2+} signal. (Middle) Normalized fluorescence response of all three signals. (Right) Scatter plot of the normalized peak amplitude of all three signals. Individual peak amplitude was normalized to the maximum peak amplitude for each sensor signal. The magenta circles indicate the correlation between DA and Ca^{2+}, while the green circles indicate the correlation between ATP and Ca^{2+}. The data were fitted with a linear function. A total of 33 peaks were selected in 3 zebrafish.
(H) Group summary of the decay kinetics of all three sensor signals measured during electrical shock (n = 8 zebrafish) or PTZ application (n = 3 zebrafish). The values were obtained by fitting the traces with a single-exponential function.

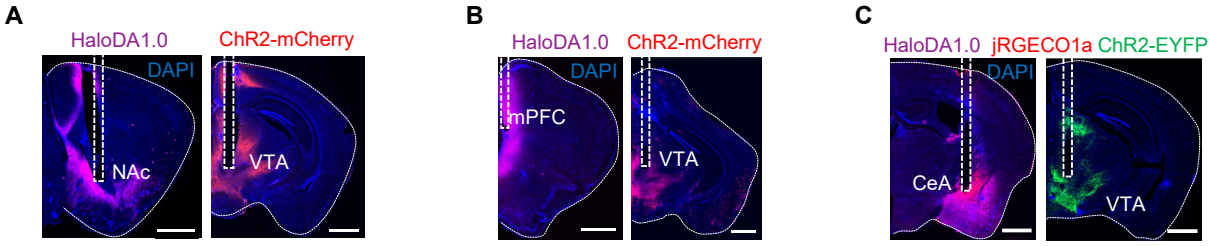

Fig. S8. Validation of optogenetic expression in mice.
Histological verification of the expression of the indicated sensors and optogenetic actuators in the VTA and NAc (**A**), VTA and mPFC (**B**), and VTA and CeA (**C**). The dashed lines indicate the location of the optical tract. Scale bars, 1 mm.

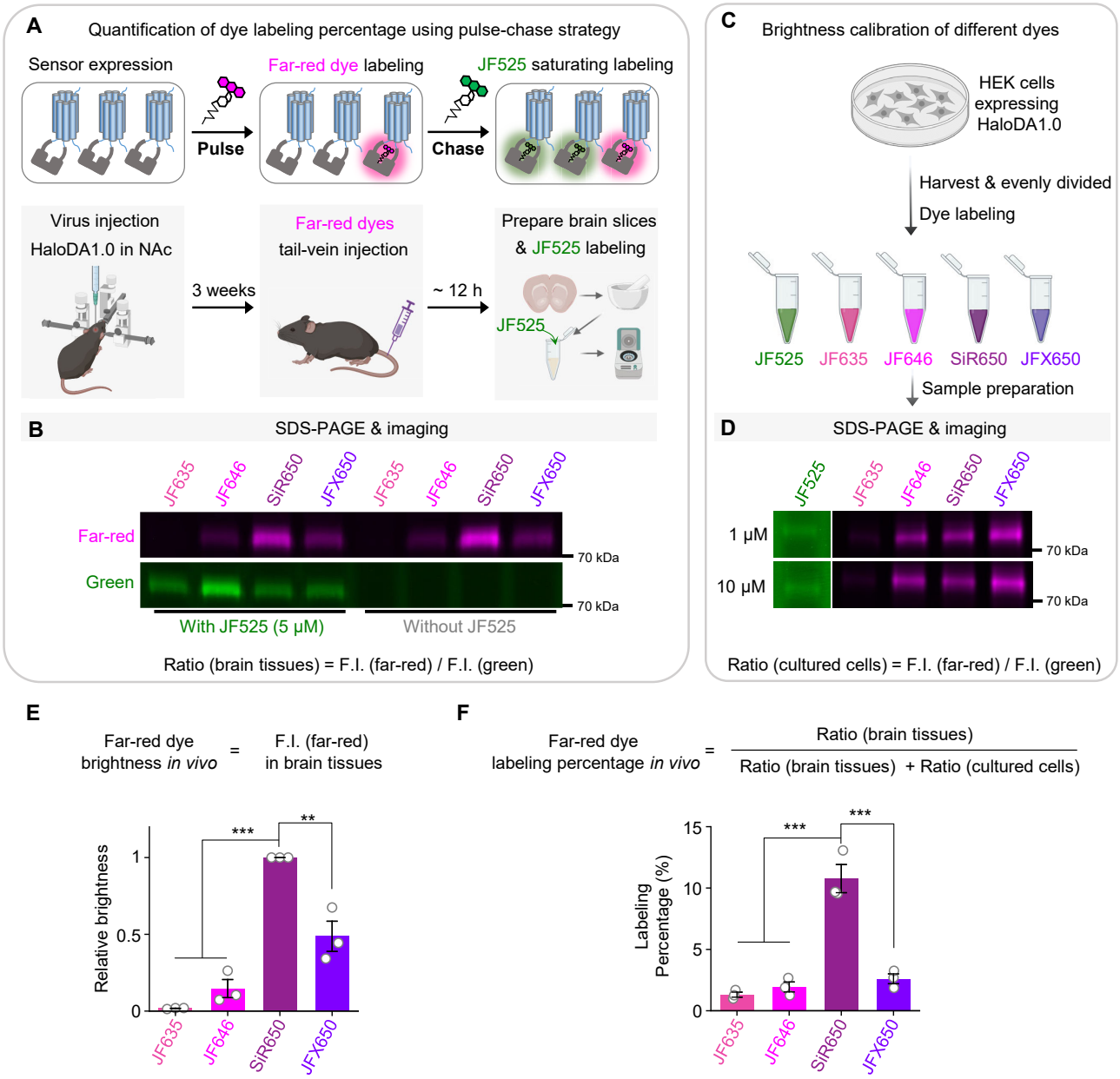

Fig. S9. Comparison of dye labeling efficiency in mice.

(**A**) chematic diagram depicting the strategy and workflow for measuring dye labeling percentage in mice.

(**B**) Representative fluorescence images of SDS-PAGE for brain tissues.

(**C**) Schematic diagram depicting the workflow for brightness calibration in cultured HEK293T cells.

(**D**) Representative fluorescence images of SDS-PAGE for cultured cells. Both 1 μM and 10 μM dye concentrations yielded comparable fluorescence intensities, confirming full labeling at both concentrations. Fluorescence images at 10 μM were used for quantification.

(**E** and **F**) Calculation formula (top) and group summary of dye brightness (**E**, bottom) and dye labeling percentage (**F**, bottom) in mice. n = 3 mice per group.

A

	EC (M^{-1} cm^{-1})	QY	Brightness (QY * EC) x 10^3
HaloTag-SiR650	167,000	0.55	92.35
EGFP	55,900	0.60	33.54
mCherry	72,000	0.22	15.84
mKate	45,000	0.33	14.85
mkelly2	43,000	0.18	7.74
mMaroon1	80,000	0.11	8.8
mIFP	82,000	0.08	6.56

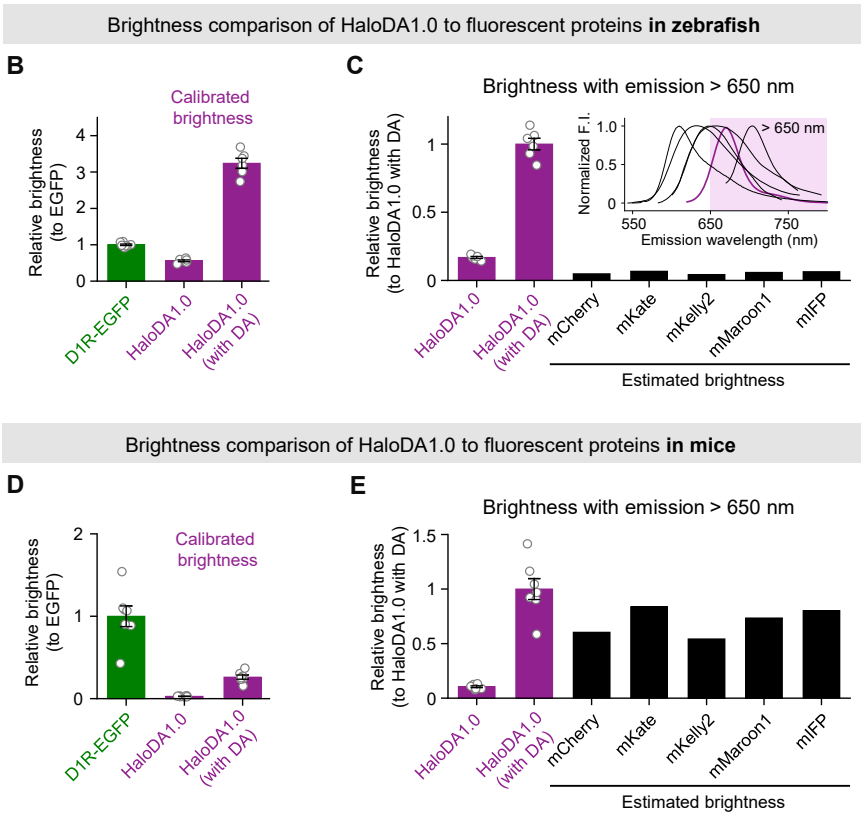

Fig. S10. Brightness comparison of HaloDA1.0-SiR650 to fluorescent proteins in zebrafish and in mice.

(**A**) eported extinction coefficient (EC), quantum yield (QY) and brightness (EC*QY) of HaloTag-SiR650(*81*) and some fluorescent proteins(*82*).

(**B**) Calibrated brightness of basal and DA-bound HaloDA1.0 relative to EGFP in zebrafish. n= 6–8 zebrafish per group.

(**C**) Comparison of the brightness of basal and DA-bound HaloDA1.0 in zebrafish with red and far-red fluorescent proteins in the far-red spectral range (emission > 650 nm). The inset shows emission spectra of HaloDA1.0-SiR650 (replotted from **Fig. S3**) and indicated fluorescent proteins(*82*).

(**D**) Calibrated brightness of basal and DA-bound HaloDA1.0 relative to EGFP in mice. The relative brightness of EGFP and HaloDA1.0-SiR650 in mice was estimated from their brightness in cultured cells and the measured HaloDA1.0-SiR650 labeling percentage in mice. n = 7 wells per group with 300–500 cells per well.

(**E**) Comparison of the brightness of basal and DA-bound HaloDA1.0 in mice with red and far-red fluorescent proteins in the far-red spectral range (emission > 650 nm).

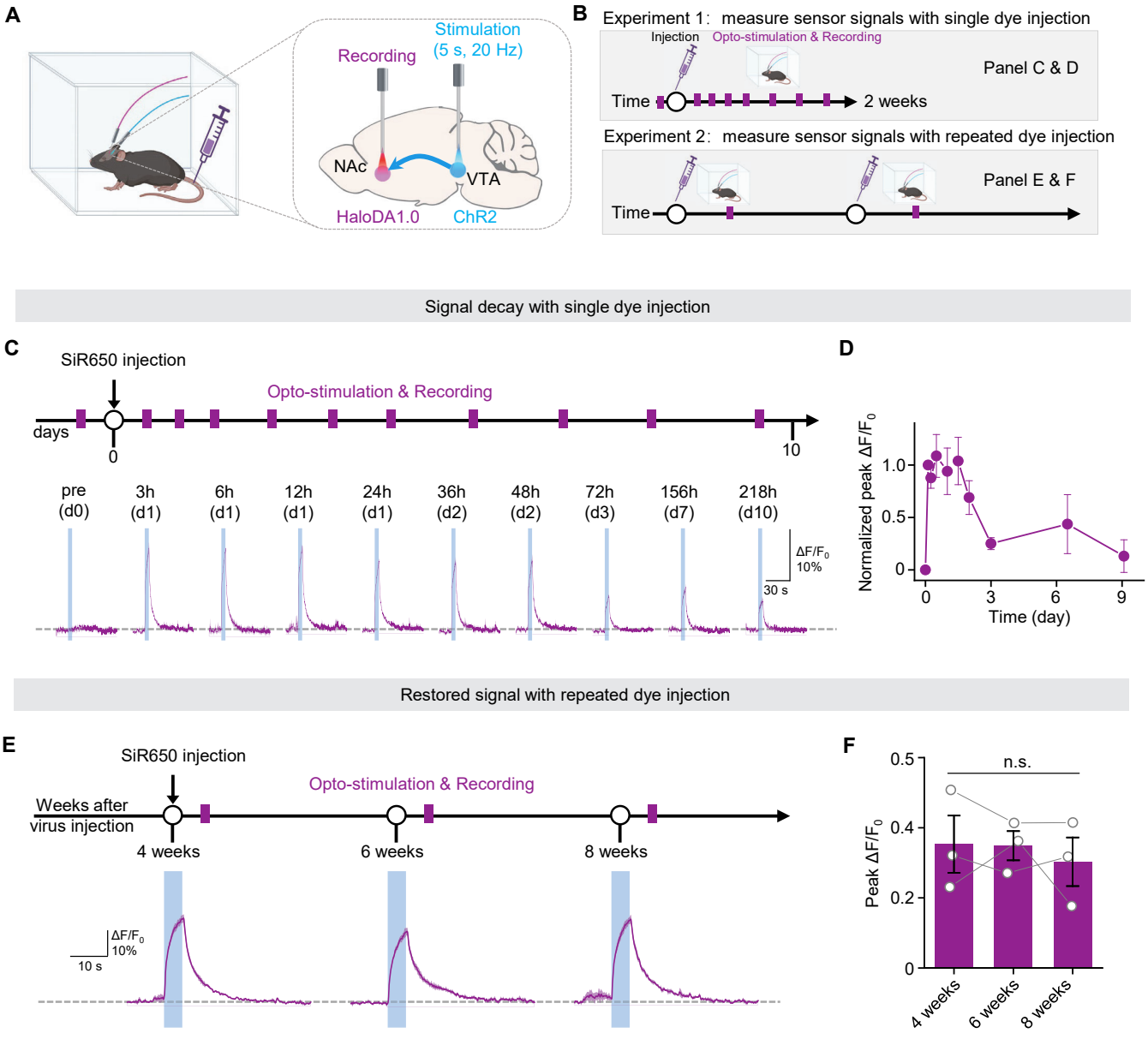

Fig. S11. Measuring sensor signals after a single or repeated dye injections.
(**A**) Schematic diagram depicting the strategy for fiber photometry recording of HaloDA1.0 in the NAc upon optogenetic stimulation of VTA neurons.
(**B**) chematic diagram depicting the experimental protocol for measuring sensor signals, with a single injection of 100 nmol SiR650 in the tail vein (experiment 1, top) or repeated injections of 100 nmol SiR650 (experiment 2, bottom).
(**C** and **D**) Representative fluorescence responses to optogenetic stimuli (**C**) and group summary of normalized peak $\Delta F/F_0$ (**D**) measured before dye injection and at the indicated time points after a single injection of dye; n = 3 mice. The vertical blue shading indicates the optogenetic stimuli.
(**E** and **F**) Representative fluorescence responses to optogenetic stimuli (**E**) and group summary of peak $\Delta F/F_0$ (**F**) measured with repeated dye injections in weeks 4, 6, and 8. Each measurement was performed 12 hours after dye injection; n = 3 mice.

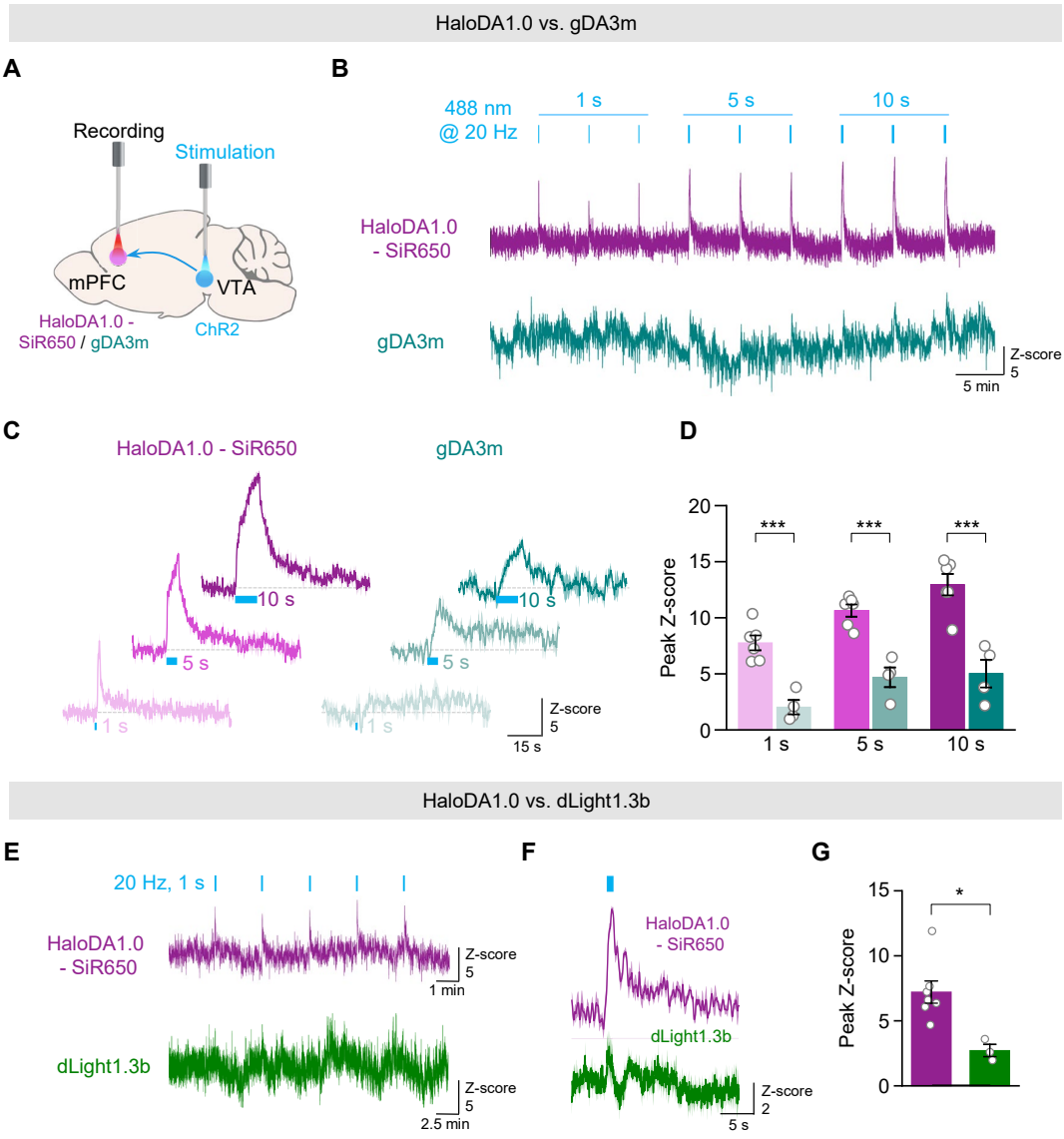

Fig. S12. *In vivo* comparison of HaloDA1.0 versus green DA sensors in the mPFC upon optogenetic stimulation.

(**A**) Schematic illustration depicting the strategy for fiber photometry recording of HaloDA1.0 and gDA3m in the mPFC upon optogenetic stimulation of VTA neurons.

(**B** to **D**) Representative traces (**B**), average traces (**C**) and group summary (**D**) of the change in fluorescence of SiR650-labeled HaloDA1.0 and gDA3m under the indicated conditions. The blue ticks indicate the optogenetic stimuli applied at 20 Hz. n= 4–6 mice per group.

(**E** to **G**) Representative traces (**E**), average traces (**F**) and group summary (**G**) of the change in fluorescence of SiR650-labeled HaloDA1.0 and dLight1.3b under the indicated conditions. n= 3–7 mice per group. The data for dLight1.3b were replotted from previously published results(*10*).

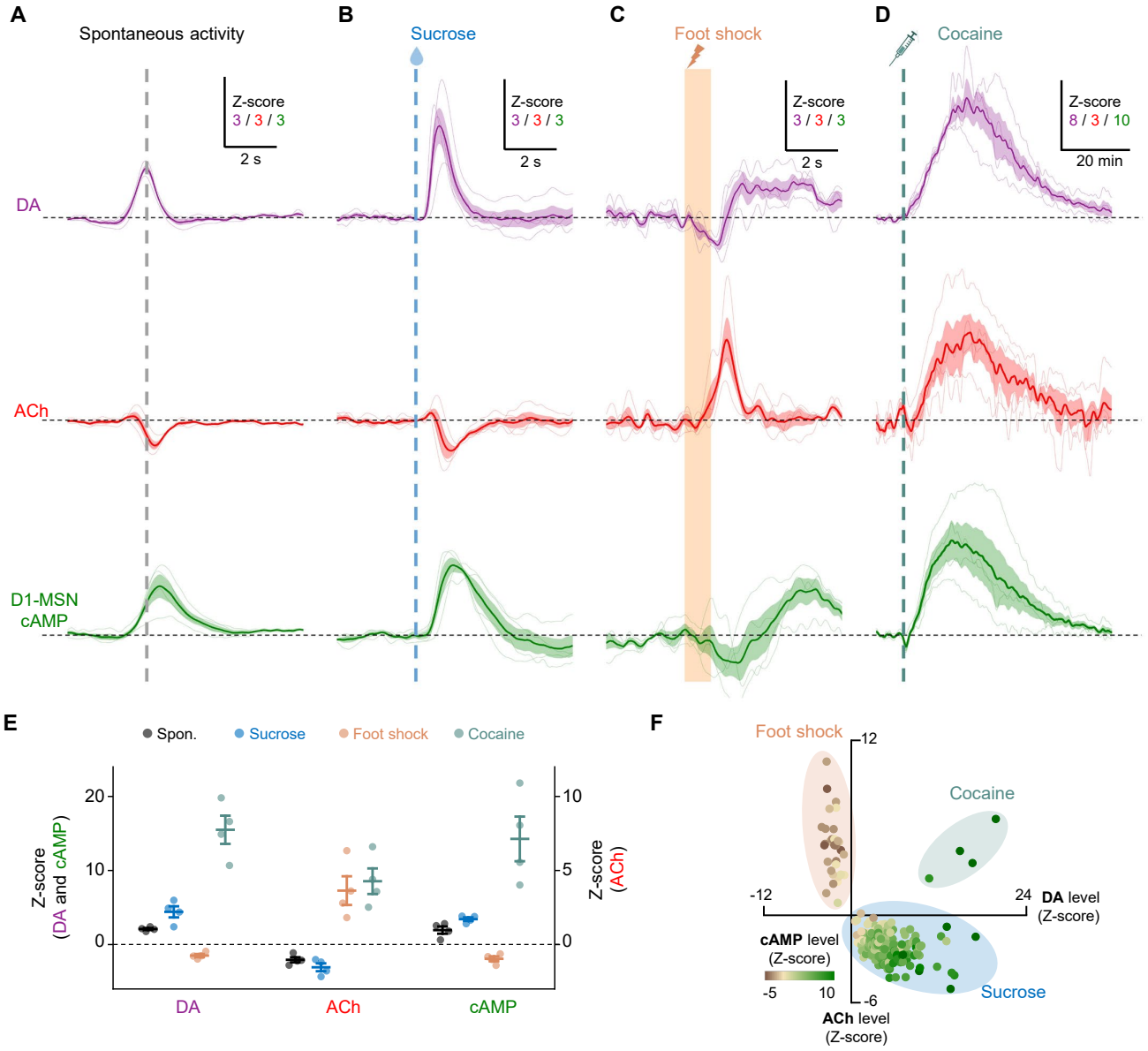

Fig. S13. Measuring the fluorescence responses of DA, ACh, and cAMP sensors *in vivo*.
(**A** to **D**) The change in fluorescence for the HaloDA1.0 (DA), rACh1h (ACh), and DIO-GFlamp2 (D1-MSN cAMP) sensors measured during spontaneous activity (**A**) and in response to sucrose (**B**), foot shock (**C**), and cocaine application (**D**). The thin traces represent the fluorescence changes measured in an individual mouse, while the thick traces indicate the average fluorescence change; n = 4 mice for each condition.
(**E**) Group summary of the peak or trough responses for all three sensor signals under the indicated conditions; n = 4 mice.
(**F**) catter plot of the peak/trough amplitude of the three sensor signals measured under the indicated conditions; n = 4 mice. Each point represents an individual trial. The ACh response is plotted on the *y*-axis, the DA response is plotted on the *x*-axis, and the color of each data point indicates the cAMP response.

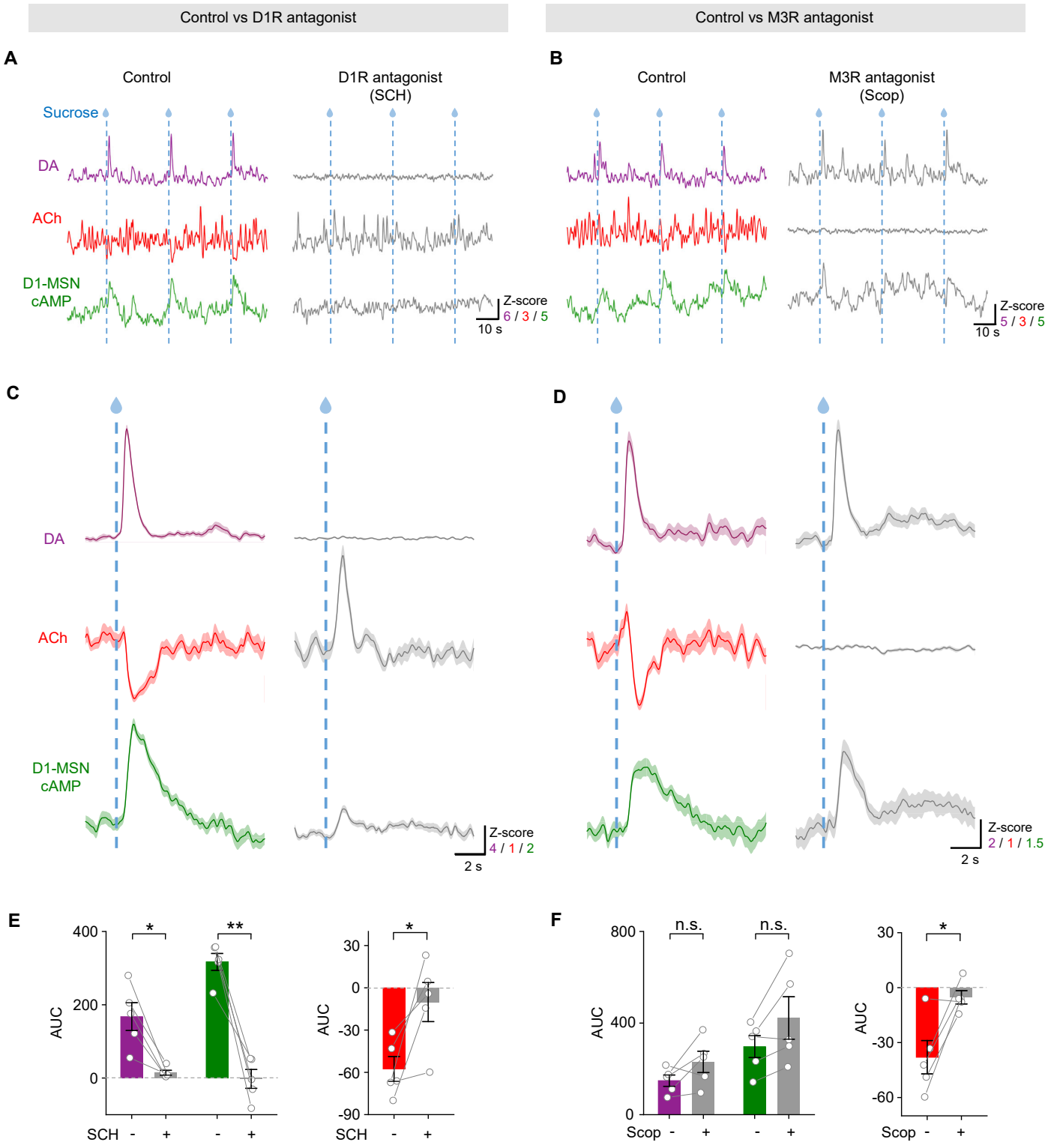

Fig. S14. Pharmacologic validation during three-color recording.
Representative traces of the change in fluorescence (**A** and **B**), average traces (**C** and **D**), and group summary of area under the curve (AUC, 0-5 s) (**E** and **F**) measured for DA, ACh and D1-MSN cAMP sensors under control conditions and following an i.p. injection of 8 mg/kg SCH (**A**, **C**, and **E**) or 10 mg/kg Scop (**B**, **D**, and **F**). n = 5 mice per group.

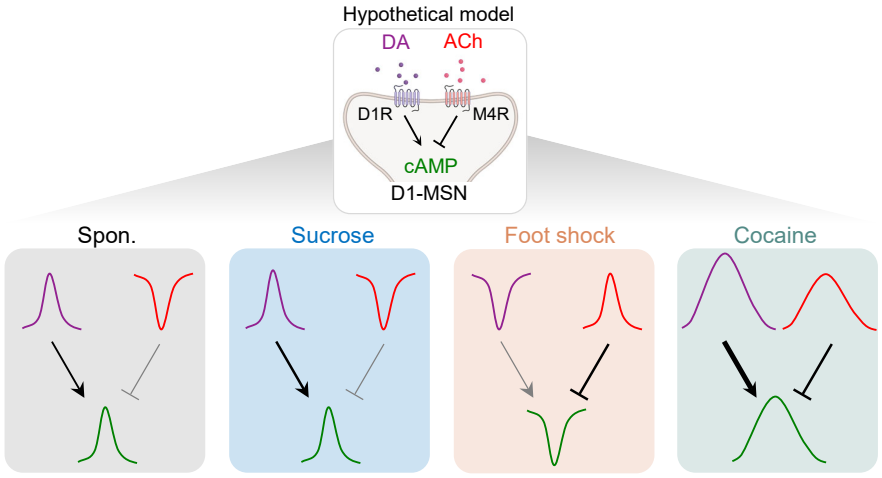

Fig. S15. Model illustrating the proposed effects of DA and ACh on D1-MSN cAMP amounts. Elevated DA and reduced ACh increase cAMP production during spontaneous activity and in response to sucrose, while decreased DA and increased ACh reduce cAMP production during foot shock. In contrast, both DA and ACh increase in response to cocaine, exerting opposing effects on cAMP production.

References and Notes

1. L. Luo, Architectures of neuronal circuits. *Science* **373**, eabg7285 (2021). doi:10.1126/science.abg7285 Medline

2. T. Sippy, N. X. Tritsch, Unraveling the dynamics of dopamine release and its actions on target cells. *Trends Neurosci.* **46**, 228–239 (2023). doi:10.1016/j.tins.2022.12.005 Medline

3. A. M. Graybiel, T. Aosaki, A. W. Flaherty, M. Kimura, The basal ganglia and adaptive motor control. *Science* **265**, 1826–1831 (1994). doi:10.1126/science.8091209 Medline

4. R. A. Wise, Dopamine, learning and motivation. *Nat. Rev. Neurosci.* **5**, 483–494 (2004). doi:10.1038/nrn1406 Medline

5. W. Schultz, P. Dayan, P. R. Montague, A neural substrate of prediction and reward. *Science* **275**, 1593–1599 (1997). doi:10.1126/science.275.5306.1593 Medline

6. D. M. Lovinger, Y. Mateo, K. A. Johnson, S. A. Engi, M. Antonazzo, J. F. Cheer, Local modulation by presynaptic receptors controls neuronal communication and behaviour. *Nat. Rev. Neurosci.* **23**, 191–203 (2022). doi:10.1038/s41583-022-00561-0 Medline

7. K. Z. Peters, J. F. Cheer, R. Tonini, Modulating the neuromodulators: Dopamine, serotonin, and the endocannabinoid system. *Trends Neurosci.* **44**, 464–477 (2021). doi:10.1016/j.tins.2021.02.001 Medline

8. S. J. Lee, B. Lodder, Y. Chen, T. Patriarchi, L. Tian, B. L. Sabatini, Cell-type-specific asynchronous modulation of PKA by dopamine in learning. *Nature* **590**, 451–456 (2021). doi:10.1038/s41586-020-03050-5 Medline

9. P. Greengard, P. B. Allen, A. C. Nairn, Beyond the dopamine receptor: The DARPP-32/protein phosphatase-1 cascade. *Neuron* **23**, 435–447 (1999). doi:10.1016/S0896-6273(00)80798-9 Medline

10. Y. Zhuo, B. Luo, X. Yi, H. Dong, X. Miao, J. Wan, J. T. Williams, M. G. Campbell, R. Cai, T. Qian, F. Li, S. J. Weber, L. Wang, B. Li, Y. Wei, G. Li, H. Wang, Y. Zheng, Y. Zhao, M. E. Wolf, Y. Zhu, M. Watabe-Uchida, Y. Li, Improved green and red GRAB sensors for monitoring dopaminergic activity in vivo. *Nat. Methods* **21**, 680–691 (2024). doi:10.1038/s41592-023-02100-w Medline

11. F. Sun, J. Zeng, M. Jing, J. Zhou, J. Feng, S. F. Owen, Y. Luo, F. Li, H. Wang, T. Yamaguchi, Z. Yong, Y. Gao, W. Peng, L. Wang, S. Zhang, J. Du, D. Lin, M. Xu, A. C. Kreitzer, G. Cui, Y. Li, A genetically encoded fluorescent sensor enables rapid and specific detection of dopamine in flies, fish, and mice. *Cell* **174**, 481–496.e19 (2018). doi:10.1016/j.cell.2018.06.042 Medline

12. T. Patriarchi, J. R. Cho, K. Merten, M. W. Howe, A. Marley, W.-H. Xiong, R. W. Folk, G. J. Broussard, R. Liang, M. J. Jang, H. Zhong, D. Dombeck, M. von Zastrow, A. Nimmerjahn, V. Gradinaru, J. T. Williams, L. Tian, Ultrafast neuronal imaging of

dopamine dynamics with designed genetically encoded sensors. *Science* **360**, eaat4422 (2018). doi:10.1126/science.aat4422 Medline

13. T. Patriarchi, A. Mohebi, J. Sun, A. Marley, R. Liang, C. Dong, K. Puhger, G. O. Mizuno, C. M. Davis, B. Wiltgen, M. von Zastrow, J. D. Berke, L. Tian, An expanded palette of dopamine sensors for multiplex imaging in vivo. *Nat. Methods* **17**, 1147–1155 (2020). doi:10.1038/s41592-020-0936-3 Medline

14. F. Sun, J. Zhou, B. Dai, T. Qian, J. Zeng, X. Li, Y. Zhuo, Y. Zhang, Y. Wang, C. Qian, K. Tan, J. Feng, H. Dong, D. Lin, G. Cui, Y. Li, Next-generation GRAB sensors for monitoring dopaminergic activity in vivo. *Nat. Methods* **17**, 1156–1166 (2020). doi:10.1038/s41592-020-00981-9 Medline

15. Z. Wu, D. Lin, Y. Li, Pushing the frontiers: Tools for monitoring neurotransmitters and neuromodulators. *Nat. Rev. Neurosci.* **23**, 257–274 (2022). doi:10.1038/s41583-022-00577-6 Medline

16. D. M. Shcherbakova, Near-infrared and far-red genetically encoded indicators of neuronal activity. *J. Neurosci. Methods* **362**, 109314 (2021). doi:10.1016/j.jneumeth.2021.109314 Medline

17. D. M. Shcherbakova, O. V. Stepanenko, K. K. Turoverov, V. V. Verkhusha, Near-infrared fluorescent proteins: Multiplexing and optogenetics across scales. *Trends Biotechnol.* **36**, 1230–1243 (2018). doi:10.1016/j.tibtech.2018.06.011 Medline

18. G. V. Los, L. P. Encell, M. G. McDougall, D. D. Hartzell, N. Karassina, C. Zimprich, M. G. Wood, R. Learish, R. F. Ohana, M. Urh, D. Simpson, J. Mendez, K. Zimmerman, P. Otto, G. Vidugiris, J. Zhu, A. Darzins, D. H. Klaubert, R. F. Bulleit, K. V. Wood, HaloTag: A novel protein labeling technology for cell imaging and protein analysis. *ACS Chem. Biol.* **3**, 373–382 (2008). doi:10.1021/cb800025k Medline

19. L. D. Lavis, Teaching old dyes new tricks: Biological probes built from fluoresceins and rhodamines. *Annu. Rev. Biochem.* **86**, 825–843 (2017). doi:10.1146/annurev-biochem-061516-044839 Medline

20. Y. Nasu, Y. Shen, L. Kramer, R. E. Campbell, Structure- and mechanism-guided design of single fluorescent protein-based biosensors. *Nat. Chem. Biol.* **17**, 509–518 (2021). doi:10.1038/s41589-020-00718-x Medline

21. L. Wang, M. Tran, E. D'Este, J. Roberti, B. Koch, L. Xue, K. Johnsson, A general strategy to develop cell permeable and fluorogenic probes for multicolour nanoscopy. *Nat. Chem.* **12**, 165–172 (2020). doi:10.1038/s41557-019-0371-1 Medline

22. J. B. Grimm, A. N. Tkachuk, L. Xie, H. Choi, B. Mohar, N. Falco, K. Schaefer, R. Patel, Q. Zheng, Z. Liu, J. Lippincott-Schwartz, T. A. Brown, L. D. Lavis, A general method to optimize and functionalize red-shifted rhodamine dyes. *Nat. Methods* **17**, 815–821 (2020). doi:10.1038/s41592-020-0909-6 Medline

23. C. Deo, A. S. Abdelfattah, H. K. Bhargava, A. J. Berro, N. Falco, H. Farrants, B. Moeyaert, M. Chupanova, L. D. Lavis, E. R. Schreiter, The HaloTag as a general scaffold for far-red tunable chemigenetic indicators. *Nat. Chem. Biol.* **17**, 718–723 (2021). doi:10.1038/s41589-021-00775-w Medline

24. L. Wang, J. Hiblot, C. Popp, L. Xue, K. Johnsson, Environmentally sensitive color-shifting fluorophores for bioimaging. *Angew. Chem. Int. Ed.* **59**, 21880–21884 (2020). doi:10.1002/anie.202008357 Medline

25. J. B. Grimm, B. P. English, J. Chen, J. P. Slaughter, Z. Zhang, A. Revyakin, R. Patel, J. J. Macklin, D. Normanno, R. H. Singer, T. Lionnet, L. D. Lavis, A general method to improve fluorophores for live-cell and single-molecule microscopy. *Nat. Methods* **12**, 244–250, 3, 250 (2015). doi:10.1038/nmeth.3256 Medline

26. J. B. Grimm, A. K. Muthusamy, Y. Liang, T. A. Brown, W. C. Lemon, R. Patel, R. Lu, J. J. Macklin, P. J. Keller, N. Ji, L. D. Lavis, A general method to fine-tune fluorophores for live-cell and in vivo imaging. *Nat. Methods* **14**, 987–994 (2017). doi:10.1038/nmeth.4403 Medline

27. G. Lukinavičius, K. Umezawa, N. Olivier, A. Honigmann, G. Yang, T. Plass, V. Mueller, L. Reymond, I. R. Corrêa Jr., Z.-G. Luo, C. Schultz, E. A. Lemke, P. Heppenstall, C. Eggeling, S. Manley, K. Johnsson, A near-infrared fluorophore for live-cell super-resolution microscopy of cellular proteins. *Nat. Chem.* **5**, 132–139 (2013). doi:10.1038/nchem.1546 Medline

28. G. Lukinavičius, L. Reymond, K. Umezawa, O. Sallin, E. D'Este, F. Göttfert, H. Ta, S. W. Hell, Y. Urano, K. Johnsson, Fluorogenic probes for multicolor imaging in living cells. *J. Am. Chem. Soc.* **138**, 9365–9368 (2016). doi:10.1021/jacs.6b04782 Medline

29. Q. Zheng, A. X. Ayala, I. Chung, A. V. Weigel, A. Ranjan, N. Falco, J. B. Grimm, A. N. Tkachuk, C. Wu, J. Lippincott-Schwartz, R. H. Singer, L. D. Lavis, Rational design of fluorogenic and spontaneously blinking labels for super-resolution imaging. *ACS Cent. Sci.* **5**, 1602–1613 (2019). doi:10.1021/acscentsci.9b00676 Medline

30. J. B. Grimm, L. Xie, J. C. Casler, R. Patel, A. N. Tkachuk, N. Falco, H. Choi, J. Lippincott-Schwartz, T. A. Brown, B. S. Glick, Z. Liu, L. D. Lavis, A general method to improve fluorophores using deuterated auxochromes. *JACS Au* **1**, 690–696 (2021). doi:10.1021/jacsau.1c00006 Medline

31. F. Deng, J. Wan, G. Li, H. Dong, X. Xia, Y. Wang, X. Li, C. Zhuang, Y. Zheng, L. Liu, Y. Yan, J. Feng, Y. Zhao, H. Xie, Y. Li, Improved green and red GRAB sensors for monitoring spatiotemporal serotonin release in vivo. *Nat. Methods* **21**, 692–702 (2024). doi:10.1038/s41592-024-02188-8 Medline

32. J. Feng, H. Dong, J. E. Lischinsky, J. Zhou, F. Deng, C. Zhuang, X. Miao, H. Wang, G. Li, R. Cai, H. Xie, G. Cui, D. Lin, Y. Li, Monitoring norepinephrine release in vivo using next-generation $GRAB_{NE}$ sensors. *Neuron* **112**, 1930–1942.e6 (2024). doi:10.1016/j.neuron.2024.03.001 Medline

33. K. Z. Peters, E. B. Oleson, J. F. Cheer, A brain on cannabinoids: The role of dopamine release in reward seeking and addiction. *Cold Spring Harb. Perspect. Med.* **11**, a039305 (2021). doi:10.1101/cshperspect.a039305 Medline

34. S. Xie, X. Miao, G. Li, Y. Zheng, M. Li, E. Ji, J. Wang, S. Li, R. Cai, L. Geng, J. Feng, C. Wei, Y. Li, Red-shifted GRAB acetylcholine sensors for multiplex imaging in vivo. bioRxiv 627112 [Preprint] (2024); https://doi.org/10.1101/2024.12.22.627112.

35. A. Dong, K. He, B. Dudok, J. S. Farrell, W. Guan, D. J. Liput, H. L. Puhl, R. Cai, H. Wang, J. Duan, E. Albarran, J. Ding, D. M. Lovinger, B. Li, I. Soltesz, Y. Li, A fluorescent sensor for spatiotemporally resolved imaging of endocannabinoid dynamics in vivo. *Nat. Biotechnol.* **40**, 787–798 (2022). doi:10.1038/s41587-021-01074-4 Medline

36. A. C. Kreitzer, W. G. Regehr, Retrograde inhibition of presynaptic calcium influx by endogenous cannabinoids at excitatory synapses onto Purkinje cells. *Neuron* **29**, 717–727 (2001). doi:10.1016/S0896-6273(01)00246-X Medline

37. T. Ohno-Shosaku, T. Maejima, M. Kano, Endogenous cannabinoids mediate retrograde signals from depolarized postsynaptic neurons to presynaptic terminals. *Neuron* **29**, 729–738 (2001). doi:10.1016/S0896-6273(01)00247-1 Medline

38. R. I. Wilson, R. A. Nicoll, Endogenous cannabinoids mediate retrograde signalling at hippocampal synapses. *Nature* **410**, 588–592 (2001). doi:10.1038/35069076 Medline

39. R. Mechoulam, L. A. Parker, The endocannabinoid system and the brain. *Annu. Rev. Psychol.* **64**, 21–47 (2013). doi:10.1146/annurev-psych-113011-143739 Medline

40. B. D. Heifets, P. E. Castillo, Endocannabinoid signaling and long-term synaptic plasticity. *Annu. Rev. Physiol.* **71**, 283–306 (2009). doi:10.1146/annurev.physiol.010908.163149 Medline

41. C. Liu, P. Goel, P. S. Kaeser, Spatial and temporal scales of dopamine transmission. *Nat. Rev. Neurosci.* **22**, 345–358 (2021). doi:10.1038/s41583-021-00455-7 Medline

42. M. Sarter, V. Parikh, W. M. Howe, Phasic acetylcholine release and the volume transmission hypothesis: Time to move on. *Nat. Rev. Neurosci.* **10**, 383–390 (2009). doi:10.1038/nrn2635 Medline

43. N. Chuhma, S. Mingote, H. Moore, S. Rayport, Dopamine neurons control striatal cholinergic neurons through regionally heterogeneous dopamine and glutamate signaling. *Neuron* **81**, 901–912 (2014). doi:10.1016/j.neuron.2013.12.027 Medline

44. C. Straub, N. X. Tritsch, N. A. Hagan, C. Gu, B. L. Sabatini, Multiphasic modulation of cholinergic interneurons by nigrostriatal afferents. *J. Neurosci.* **34**, 8557–8569 (2014). doi:10.1523/JNEUROSCI.0589-14.2014 Medline

45. S. Wieland, D. Du, M. J. Oswald, R. Parlato, G. Köhr, W. Kelsch, Phasic dopaminergic activity exerts fast control of cholinergic interneuron firing through sequential

NMDA, D2, and D1 receptor activation. *J. Neurosci.* **34**, 11549–11559 (2014). doi:10.1523/JNEUROSCI.1175-14.2014 Medline

46. C. Liu, X. Cai, A. Ritzau-Jost, P. F. Kramer, Y. Li, Z. M. Khaliq, S. Hallermann, P. S. Kaeser, An action potential initiation mechanism in distal axons for the control of dopamine release. *Science* **375**, 1378–1385 (2022). doi:10.1126/science.abn0532 Medline

47. F.-M. Zhou, Y. Liang, J. A. Dani, Endogenous nicotinic cholinergic activity regulates dopamine release in the striatum. *Nat. Neurosci.* **4**, 1224–1229 (2001). doi:10.1038/nn769 Medline

48. S. Threlfell, T. Lalic, N. J. Platt, K. A. Jennings, K. Deisseroth, S. J. Cragg, Striatal dopamine release is triggered by synchronized activity in cholinergic interneurons. *Neuron* **75**, 58–64 (2012). doi:10.1016/j.neuron.2012.04.038 Medline

49. Z. Wu, K. He, Y. Chen, H. Li, S. Pan, B. Li, T. Liu, F. Xi, F. Deng, H. Wang, J. Du, M. Jing, Y. Li, A sensitive GRAB sensor for detecting extracellular ATP in vitro and in vivo. *Neuron* **110**, 770–782.e5 (2022). doi:10.1016/j.neuron.2021.11.027 Medline

50. B. Mohar, G. Michel, Y.-Z. Wang, V. Hernandez, J. B. Grimm, J.-Y. Park, R. Patel, M. Clarke, T. A. Brown, C. Bergmann, K. K. Gebis, A. P. Wilen, B. Liu, R. Johnson, A. Graves, T. Tchumatchenko, J. N. Savas, E. F. Fornasiero, R. L. Huganir, P. W. Tillberg, L. D. Lavis, K. Svoboda, N. Spruston, DELTA: A method for brain-wide measurement of synaptic protein turnover reveals localized plasticity during learning. *Nat. Neurosci.* **28**, 1089-1098 (2025). doi:10.1038/s41593-025-01923-4 Medline

51. E. Bulovaite, Z. Qiu, M. Kratschke, A. Zgraj, D. G. Fricker, E. J. Tuck, R. Gokhale, B. Koniaris, S. A. Jami, P. Merino-Serrais, E. Husi, L. Mendive-Tapia, M. Vendrell, T. J. O'Dell, J. DeFelipe, N. H. Komiyama, A. Holtmaat, E. Fransén, S. G. N. Grant, A brain atlas of synapse protein lifetime across the mouse lifespan. *Neuron* **110**, 4057–4073.e8 (2022). doi:10.1016/j.neuron.2022.09.009 Medline

52. K. Yamaguchi, S. Inoue, O. Ohara, T. Nagase, "Pulse-chase experiment for the analysis of protein stability in cultured mammalian cells by covalent fluorescent labeling of fusion proteins" in *Reverse Chemical Genetics*, H. Koga, Ed. (Humana Press, 2009), pp. 121–131.

53. K. T. Beier, E. E. Steinberg, K. E. DeLoach, S. Xie, K. Miyamichi, L. Schwarz, X. J. Gao, E. J. Kremer, R. C. Malenka, L. Luo, Circuit architecture of VTA dopamine neurons revealed by systematic input-output mapping. *Cell* **162**, 622–634 (2015). doi:10.1016/j.cell.2015.07.015 Medline

54. K. Abe, Y. Kambe, K. Majima, Z. Hu, M. Ohtake, A. Momennezhad, H. Izumi, T. Tanaka, A. Matunis, E. Stacy, T. Itokazu, T. R. Sato, T. Sato, Functional diversity of dopamine axons in prefrontal cortex during classical conditioning. *eLife* **12**, RP91136 (2024). doi:10.7554/eLife.91136.3 Medline

55. R. A. Phillips 3rd, J. J. Tuscher, S. L. Black, E. Andraka, N. D. Fitzgerald, L. Ianov, J. J. Day, An atlas of transcriptionally defined cell populations in the rat ventral tegmental area. *Cell Rep.* **39**, 110616 (2022). doi:10.1016/j.celrep.2022.110616 Medline

56. B. Yaghmaeian Salmani, L. Lahti, L. Gillberg, J. K. Jacobsen, I. Mantas, P. Svenningsson, T. Perlmann, Transcriptomic atlas of midbrain dopamine neurons uncovers differential vulnerability in a parkinsonism lesion model. *eLife* **12**, RP89482 (2024). doi:10.7554/eLife.89482.3 Medline

57. E. Casey, M. E. Avale, A. Kravitz, M. Rubinstein, Dopaminergic innervation at the central nucleus of the amygdala reveals distinct topographically segregated regions. *Brain Struct. Funct.* **228**, 663–675 (2023). doi:10.1007/s00429-023-02614-1 Medline

58. E. Casey, M. E. Avale, A. Kravitz, M. Rubinstein, Partial ablation of postsynaptic dopamine D2 receptors in the central nucleus of the amygdala increases risk avoidance in exploratory tasks. *eNeuro* **9**, ENEURO.528-21.2022 (2022). doi:10.1523/ENEURO.0528-21.2022 Medline

59. E. J. Nunes, N. A. Addy, P. J. Conn, D. J. Foster, Targeting the actions of muscarinic receptors on dopamine systems: New strategies for treating neuropsychiatric disorders. *Annu. Rev. Pharmacol. Toxicol.* **64**, 277–289 (2024). doi:10.1146/annurev-pharmtox-051921-023858 Medline

60. S. E. Yohn, P. J. Weiden, C. C. Felder, S. M. Stahl, Muscarinic acetylcholine receptors for psychotic disorders: Bench-side to clinic. *Trends Pharmacol. Sci.* **43**, 1098–1112 (2022). doi:10.1016/j.tips.2022.09.006 Medline

61. A. G. Nair, L. R. V. Castro, M. El Khoury, V. Gorgievski, B. Giros, E. T. Tzavara, J. Hellgren-Kotaleski, P. Vincent, The high efficacy of muscarinic M4 receptor in D1 medium spiny neurons reverses striatal hyperdopaminergia. *Neuropharmacology* **146**, 74–83 (2019). doi:10.1016/j.neuropharm.2018.11.029 Medline

62. N. J. Bruce, D. Narzi, D. Trpevski, S. C. van Keulen, A. G. Nair, U. Röthlisberger, R. C. Wade, P. Carloni, J. Hellgren Kotaleski, Regulation of adenylyl cyclase 5 in striatal neurons confers the ability to detect coincident neuromodulatory signals. *PLOS Comput. Biol.* **15**, e1007382 (2019). doi:10.1371/journal.pcbi.1007382 Medline

63. W. Shen, J. L. Plotkin, V. Francardo, W. K. D. Ko, Z. Xie, Q. Li, T. Fieblinger, J. Wess, R. R. Neubig, C. W. Lindsley, P. J. Conn, P. Greengard, E. Bezard, M. A. Cenci, D. J. Surmeier, M4 muscarinic receptor signaling ameliorates striatal plasticity deficits in models of L-DOPA-induced dyskinesia. *Neuron* **88**, 762–773 (2015). doi:10.1016/j.neuron.2015.10.039 Medline

64. L. Chantranupong, C. C. Beron, J. A. Zimmer, M. J. Wen, W. Wang, B. L. Sabatini, Dopamine and glutamate regulate striatal acetylcholine in decision-making. *Nature* **621**, 577–585 (2023). doi:10.1038/s41586-023-06492-9 Medline

65. A. C. Krok, M. Maltese, P. Mistry, X. Miao, Y. Li, N. X. Tritsch, Intrinsic dopamine and acetylcholine dynamics in the striatum of mice. *Nature* **621**, 543–549 (2023). doi:10.1038/s41586-023-05995-9 Medline

66. L. Wang, C. Wu, W. Peng, Z. Zhou, J. Zeng, X. Li, Y. Yang, S. Yu, Y. Zou, M. Huang, C. Liu, Y. Chen, Y. Li, P. Ti, W. Liu, Y. Gao, W. Zheng, H. Zhong, S. Gao, Z. Lu, P.-G. Ren, H. L. Ng, J. He, S. Chen, M. Xu, Y. Li, J. Chu, A high-performance genetically encoded fluorescent indicator for in vivo cAMP imaging. *Nat. Commun.* **13**, 5363 (2022). doi:10.1038/s41467-022-32994-7 Medline

67. W. Liu, C. Liu, P.-G. Ren, J. Chu, L. Wang, An improved genetically encoded fluorescent cAMP indicator for sensitive cAMP imaging and fast drug screening. *Front. Pharmacol.* **13**, 902290 (2022). doi:10.3389/fphar.2022.902290 Medline

68. Y. Zheng, Y. Li, Past, present, and future of tools for dopamine detection. *Neuroscience* **525**, 13–25 (2023). doi:10.1016/j.neuroscience.2023.06.025 Medline

69. D. Hilger, M. Masureel, B. K. Kobilka, Structure and dynamics of GPCR signaling complexes. *Nat. Struct. Mol. Biol.* **25**, 4–12 (2018). doi:10.1038/s41594-017-0011-7 Medline

70. B. T. DeVree, J. P. Mahoney, G. A. Vélez-Ruiz, S. G. F. Rasmussen, A. J. Kuszak, E. Edwald, J.-J. Fung, A. Manglik, M. Masureel, Y. Du, R. A. Matt, E. Pardon, J. Steyaert, B. K. Kobilka, R. K. Sunahara, Allosteric coupling from G protein to the agonist-binding pocket in GPCRs. *Nature* **535**, 182–186 (2016). doi:10.1038/nature18324 Medline

71. P. J. Conn, A. Christopoulos, C. W. Lindsley, Allosteric modulators of GPCRs: A novel approach for the treatment of CNS disorders. *Nat. Rev. Drug Discov.* **8**, 41–54 (2009). doi:10.1038/nrd2760 Medline

72. A. S. Abdelfattah, J. Zheng, A. Singh, Y.-C. Huang, D. Reep, G. Tsegaye, A. Tsang, B. J. Arthur, M. Rehorova, C. V. L. Olson, Y. Shuai, L. Zhang, T.-M. Fu, D. E. Milkie, M. V. Moya, T. D. Weber, A. L. Lemire, C. A. Baker, N. Falco, Q. Zheng, J. B. Grimm, M. C. Yip, D. Walpita, M. Chase, L. Campagnola, G. J. Murphy, A. M. Wong, C. R. Forest, J. Mertz, M. N. Economo, G. C. Turner, M. Koyama, B.-J. Lin, E. Betzig, O. Novak, L. D. Lavis, K. Svoboda, W. Korff, T.-W. Chen, E. R. Schreiter, J. P. Hasseman, I. Kolb, Sensitivity optimization of a rhodopsin-based fluorescent voltage indicator. *Neuron* **111**, 1547–1563.e9 (2023). doi:10.1016/j.neuron.2023.03.009 Medline

73. A. S. Abdelfattah, T. Kawashima, A. Singh, O. Novak, H. Liu, Y. Shuai, Y.-C. Huang, L. Campagnola, S. C. Seeman, J. Yu, J. Zheng, J. B. Grimm, R. Patel, J. Friedrich, B. D. Mensh, L. Paninski, J. J. Macklin, G. J. Murphy, K. Podgorski, B.-J. Lin, T.-W. Chen, G. C. Turner, Z. Liu, M. Koyama, K. Svoboda, M. B. Ahrens, L. D. Lavis, E. R. Schreiter, Bright and photostable chemigenetic indicators for extended in vivo voltage imaging. *Science* **365**, 699–704 (2019). doi:10.1126/science.aav6416 Medline

74. H. Farrants, Y. Shuai, W. C. Lemon, C. Monroy Hernandez, D. Zhang, S. Yang, R. Patel, G. Qiao, M. S. Frei, S. E. Plutkis, J. B. Grimm, T. L. Hanson, F. Tomaska, G. C. Turner, C. Stringer, P. J. Keller, A. G. Beyene, Y. Chen, Y. Liang, L. D. Lavis, E. R. Schreiter, A modular chemigenetic calcium indicator for multiplexed in vivo functional imaging. *Nat. Methods* **21**, 1916–1925 (2024). doi:10.1038/s41592-024-02411-6 Medline

75. S. Nonomura, K. Nishizawa, Y. Sakai, Y. Kawaguchi, S. Kato, M. Uchigashima, M. Watanabe, K. Yamanaka, K. Enomoto, S. Chiken, H. Sano, S. Soma, J. Yoshida, K. Samejima, M. Ogawa, K. Kobayashi, A. Nambu, Y. Isomura, M. Kimura, Monitoring and updating of action selection for goal-directed behavior through the striatal direct and indirect pathways. *Neuron* **99**, 1302–1314.e5 (2018). doi:10.1016/j.neuron.2018.08.002 Medline

76. J. Jeon, D. Dencker, G. Wörtwein, D. P. D. Woldbye, Y. Cui, A. A. Davis, A. I. Levey, G. Schütz, T. N. Sager, A. Mørk, C. Li, C.-X. Deng, A. Fink-Jensen, J. Wess, A subpopulation of neuronal M_4 muscarinic acetylcholine receptors plays a critical role in modulating dopamine-dependent behaviors. *J. Neurosci.* **30**, 2396–2405 (2010). doi:10.1523/JNEUROSCI.3843-09.2010 Medline

77. W. Wu, K. Yan, Z. He, L. Zhang, Y. Dong, B. Wu, H. Liu, S. Wang, F. Zhang, 2X-rhodamine: A bright and fluorogenic scaffold for developing near-infrared chemigenetic indicators. *J. Am. Chem. Soc.* **146**, jacs.4c03485 (2024). doi:10.1021/jacs.4c03485 Medline

78. A. Keppler, S. Gendreizig, T. Gronemeyer, H. Pick, H. Vogel, K. Johnsson, A general method for the covalent labeling of fusion proteins with small molecules in vivo. *Nat. Biotechnol.* **21**, 86–89 (2003). doi:10.1038/nbt765 Medline

79. J. Mo, J. Chen, Y. Shi, J. Sun, Y. Wu, T. Liu, J. Zhang, Y. Zheng, Y. Li, Z. Chen, Third-generation covalent TMP-tag for fast labeling and multiplexed imaging of cellular proteins. *Angew. Chem. Int. Ed.* **61**, e202207905 (2022). doi:10.1002/anie.202207905 Medline

80. J. Abramson, J. Adler, J. Dunger, R. Evans, T. Green, A. Pritzel, O. Ronneberger, L. Willmore, A. J. Ballard, J. Bambrick, S. W. Bodenstein, D. A. Evans, C.-C. Hung, M. O'Neill, D. Reiman, K. Tunyasuvunakool, Z. Wu, A. Žemgulytė, E. Arvaniti, C. Beattie, O. Bertolli, A. Bridgland, A. Cherepanov, M. Congreve, A. I. Cowen-Rivers, A. Cowie, M. Figurnov, F. B. Fuchs, H. Gladman, R. Jain, Y. A. Khan, C. M. R. Low, K. Perlin, A. Potapenko, P. Savy, S. Singh, A. Stecula, A. Thillaisundaram, C. Tong, S. Yakneen, E. D. Zhong, M. Zielinski, A. Žídek, V. Bapst, P. Kohli, M. Jaderberg, D. Hassabis, J. M. Jumper, Accurate structure prediction of biomolecular interactions with AlphaFold 3. *Nature* **630**, 493–500 (2024). doi:10.1038/s41586-024-07487-w Medline

81. M. S. Frei, M. Tarnawski, M. J. Roberti, B. Koch, J. Hiblot, K. Johnsson, Engineered HaloTag variants for fluorescence lifetime multiplexing. *Nat. Methods* **19**, 65–70 (2022). doi:10.1038/s41592-021-01341-x Medline

82. T. J. Lambert, FPbase: A community-editable fluorescent protein database. *Nat. Methods* **16**, 277–278 (2019). doi:10.1038/s41592-019-0352-8 Medline